Journal of Medicinal Chemistry

pubs.acs.org/jmc

Article

New LsrK Ligands as AI-2 Quorum Sensing Interfering Compounds against Biofilm Formation

Giorgio Milli, Angelica Pellegrini, Roberta Listro, Marina Fasolini, Katiuscia Pagano, Laura Ragona, Giampiero Pietrocola,* Pasquale Linciano,* and Simona Collina

Cite This: *J. Med. Chem.* 2024, 67, 18139−18156

Read Online

ACCESS | Metrics & More | Article Recommendations | Supporting Information

ABSTRACT: Antimicrobial resistance (AMR) represents a critical global health crisis. An innovative strategy to deal with AMR is to interfere with biofilm formation and bacterial quorum sensing (QS). In this study, newly designed autoinducer-2 (AI-2)-inspired compounds in targeting biofilm-associated infections were evaluated for their ability to inhibit biofilm formation in *Staphylococcus aureus* and *Pseudomonas aeruginosa*. The most effective compounds, **5d**, **5e**, and **7b**, exhibited potent antibiofilm activity with minimal inhibitory concentrations in the low microgram per mL range. Detailed biological assays confirmed that the antibiofilm activity was primarily driven through AI-2 QS inhibition rather than direct antimicrobial effects. The combination of different spectroscopic techniques, such as differential scanning fluorimetry, intrinsic tryptophan fluorescence, circular dichroism, and nuclear magnetic resonance, elucidated the binding between the compounds and the LsrK enzyme, a key player in AI-2 mediated QS. Our findings highlight the potential of these novel QS inhibitors as promising therapeutic agents against biofilm-associated infections.

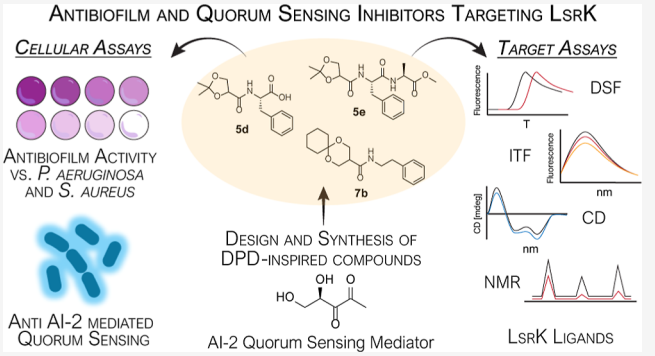

INTRODUCTION

Antimicrobial resistance (AMR) undermines the efficacy of life-saving antimicrobial treatments and has emerged as a challenging global health crisis in the contemporary medical landscape, profoundly threatening our ability to treat infectious diseases.[1] AMR is progressively becoming the major cause of morbidity and mortality worldwide, particularly in developing countries. This growing threat demands urgent action from global health authorities, healthcare providers, the pharmaceutical industry, and individuals. Investment in the development of new and effective antibiotics or mainly in new antimicrobial strategies has become mandatory.[2]

At the molecular level, the genesis of AMR can be attributed to various mechanisms employed by bacteria to defend themselves from the action of antibiotics.[3] These include the alteration of drug targets, enzymatic drug degradation, changes in cell permeability, the efflux pump mechanism, and adaptive responses like biofilm formation.[3,4] The formation of a biofilm is a complex process orchestrated by a series of genetic and environmental factors. Individual bacteria within a biofilm adhere to surfaces, secrete a matrix of extracellular polymeric substances, and undergo phenotypic changes that promote their collective survival.[5] This organized structure provides a shelter for bacteria. Bacteria organized in a biofilm are more pathogenic and able to resist antimicrobial drugs and the host immune system rather than in the planktonic stage.[6] Indeed, biofilm formation is the major component of several threatening infectious diseases in humans such as cystic fibrosis (CF) lung infections, chronic wound infections, urinary tract infections (UTIs), osteomyelitis, endocarditis, dental plaque and periodontal disease, otitis, chronic sinusitis, prosthetic joint infections, catheter-associated urinary tract infections, and ventral surgical site infections just to name a few.[7,8] *Pseudomonas aeruginosa* and *Staphylococcus aureus* are two of the most common bacterial species associated with the aforementioned infectious diseases. *P. aeruginosa*, a Gram-negative bacterium, is an opportunistic human pathogen, especially dangerous to CF patients and burn infections.[9] It is known for its ability to survive in harsh environments, including hospitals, where it can spread easily among patients and healthcare workers, and it is acquiring extensive resistance to a wide range of antibiotics.[10] *S. aureus* is a Gram-positive bacterium commonly found on the skin and mucosa of healthy individuals. Particularly methicillin-resistant *S. aureus* (MRSA) is a dangerous strain of *S. aureus* that has acquired resistance to

Received: June 3, 2024
Revised: September 18, 2024
Accepted: September 26, 2024
Published: October 9, 2024

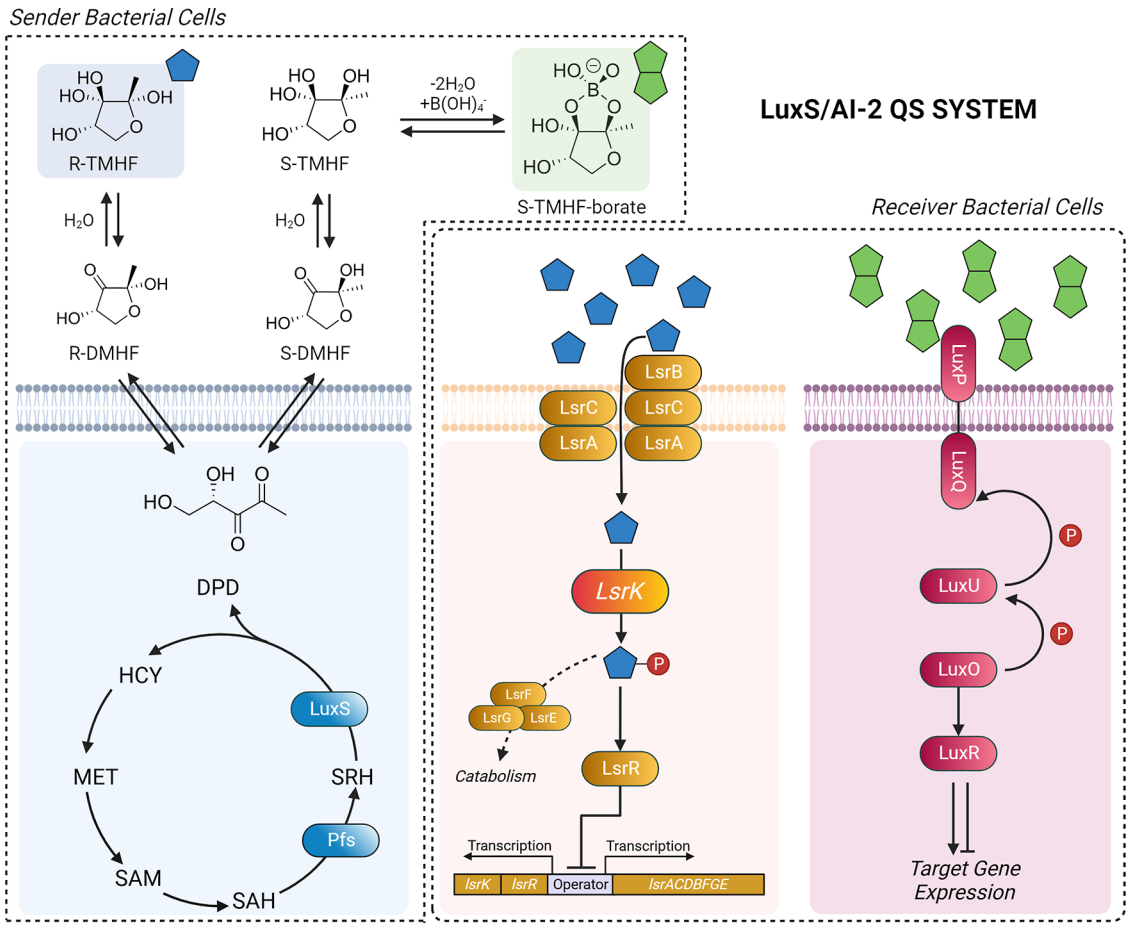

Figure 1. Regulation mechanism in the LuxS/AI-2 QS system.

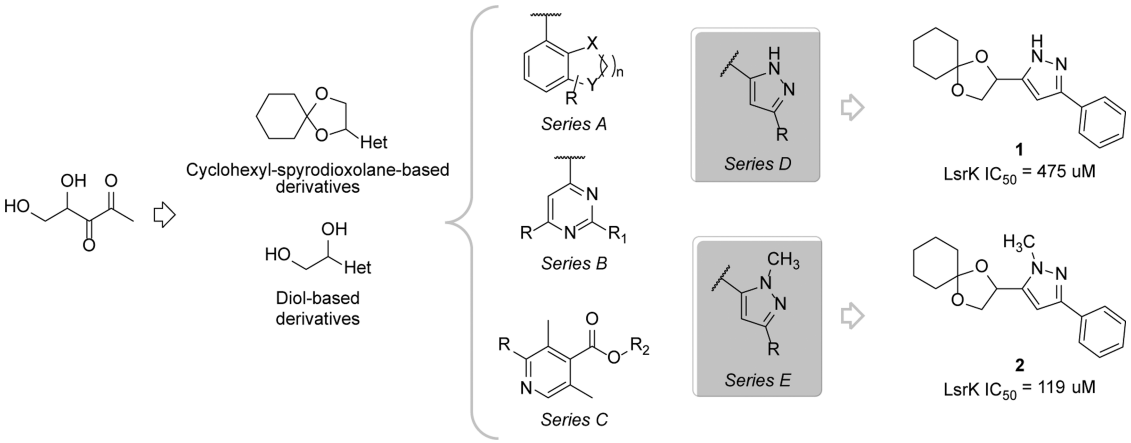

Figure 2. DPD-inspired heterocyclic compounds.

methicillin, a penicillin-type antibiotic that was once the main treatment for *S. aureus* infections. Moreover, the ability of both *P. aeruginosa* and *S. aureus* to form robust biofilms is at the basis of their pathogenesis and a critical factor in their adaptive resistance mechanisms, including the resistance to antimicrobics, significantly complicating the treatment of infections, and contributing to the global challenge of AMR.[11,12] At the heart of biofilm formation in these and other bacterial species, there is the intricate bacterial cell-to-cell communication system, known as quorum sensing (QS). Bacteria can exploit diverse QS systems, such as autoinducer-1 (AI-1), autoinducer-2 (AI-2) and oligopeptides.[13−15] AI-2 is of particular interest since it is a universal signaling molecule that mediates inter- and intraspecies QS systems among different bacteria.[16−18] AI-2 denotes a group of 4,5-dihydroxy-2,3-pentanedione (DPD) compounds that interconvert rapidly. The synthesis and detection of AI-2 by bacterial cells is resumed in Figure 1.[19] Two different executive biochemical pathways mediated by the Lsr or Lux systems can trigger the AI-2 mediated response in the receiver bacterial cell. Several studies proved the key role of the kinase LsrK in triggering the AI-2-mediated QS cascade.[20−24] LsrK is responsible for the phosphorylation of

https://doi.org/10.1021/acs.jmedchem.4c01266
J. Med. Chem. 2024, 67, 18139−18156

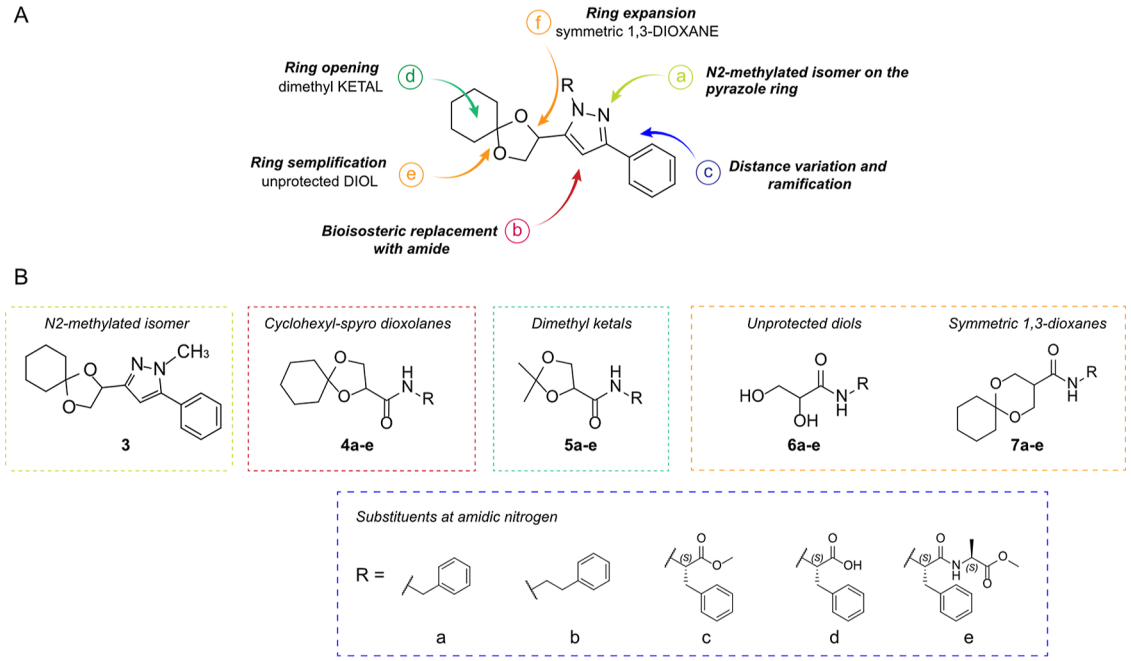

Figure 3. (A) Modifications introduced in the core structure of compound **1** and **2**. (B) Chemical structures of the newly designed compounds.

AI-2 to phospho-4,5-dihydroxy-2,3-pentanedione (P-DPD).[21,25] P-DPD binds to the transcriptional repressor LsrR, which dissociates from the promoter region of the *lsrRK* and *lsrACDBFGE* operons inducing the transcription of genes involved in biofilm formation,[26] conjugation, virulence, and antibiotic resistance[27] and in the autosustainment of QS (Figure 1).[28]

AI-2 synthesis occurs through the transformation of *S*-adenosylhomocysteine (SAH) into homocysteine, which is mediated by SAH nucleosidase (Pfs) and LuxS. LuxS is found in a broad spectrum of both Gram-negative and Gram-positive bacteria. LuxS specifically catalyzes the conversion of SRH, resulting in the production of DPD. DPD can then rearrange into *R*- or *S*-2-methyl-2,3,3,4-tetrahydroxytetrahydrofuran (*R*- or *S*-THMF), collectively known as AI-2.[29]

Recent research has demonstrated that targeting the AI-2 QS system with quorum sensing inhibitors (QSIs) able to interfere with the activity of DPD/AI-2 may be a suitable/effective approach to combat biofilm-associated infections[15,30−34] such as the ones caused by *P. aeruginosa* and *S. aureus*.[35]

In a previous work, we analyzed the ability of a small number of heterocyclic DPD derivatives to inhibit LsrK. Among them, compounds **1** and **2** (Figure 2) were found to be LsrK inhibitors with IC_{50} in the low micromolar range.[36]

In the present work, we expanded the chemical space around compounds **1**−**2**, preparing a new series counting 21 DPD-based derivatives. All compounds were tested in a cell-based assay for their capability to inhibit the biofilm formation in both *S. aureus* and *P. aeruginosa* bacterial strains, which were assumed to be representative of Gram-positive and Gram-negative bacterial species, respectively. The best-performing compounds were further characterized to assess whether the antibiofilm activity of the tested compounds is mediated through QS inhibition rather than direct antimicrobial action. In addition, due to the key role covered by LsrK in the AI-2 QS system, the ligand−LsrK binding was evaluated through diverse and complementary spectroscopic approaches, i.e., differential scanning fluorimetry (DSF), intrinsic tryptophan fluorescence spectroscopy (ITF), circular dichroism (CD), and nuclear magnetic resonance (NMR). NMR approaches based on ligand resonances observation highlighting differences in relaxation rates ^{1}H line-broadening experiments[37,38] or in saturation transfer from the protein (saturation transfer differences (STD) experiments)[38] allowed us to estimate the affinity range and map the protons of the compounds establishing key interactions with LsrK.

RESULTS AND DISCUSSION

Design. We expand the chemical space around compounds **1** and **2** by investigating the role of substitutions around the pyrazole ring as well as the cyclohexylspirodioxolane moiety and aromatic tail to fine-tune the potency of this series (Figure 3). Accordingly, 21 new DPD-based compounds (**3**, **4a**−**e**, **5a**−**e**, **6a**−**e**, and **7a**−**e**) were designed and prepared.

Briefly, compound **3** was conceived as an N2-methylated isomer in the pyrazole ring of compound **2**. Besides, the main significant modification introduced in compound **1**−**3** involved the bioisosteric substitution of the pyrazole with an amide linkage (**4a**−**e**). The cyclohexylspirodioxolane core was initially retained unchanged. Concurrently, we examined the effects of altering the proximity of the benzene ring to the cyclohexylspirodioxolane core by exploiting benzylamine (**4a**) and phenylethylamine (**4b**) or by substituting it with the aromatic system of phenylalanine (**4c**). In particular, the introduction of phenylalanine also served to add a carboxylic acid (**4d**) as a second derivatization point, thus facilitating further molecular expansion. In an exploratory step, the dipeptide Phe-Ala-COOMe was initially evaluated (**4e**). Moreover, the importance and role of the spirodioxolane moiety were investigated through various structural modifications, such as (i) replacing the bulky, hydrophobic cyclohexyl moiety with a smaller, more polar dimethyl ketal (**5a**−**e**); (ii) eliminating altogether the dioxolane system to yield the free diol (**6a**−**e**), more closely resembling the structure of DPD; and (iii) expanding the dioxolane ring into a 1,3-dioxane

https://doi.org/10.1021/acs.jmedchem.4c01266
J. Med. Chem. 2024, 67, 18139−18156

Scheme 1[a]

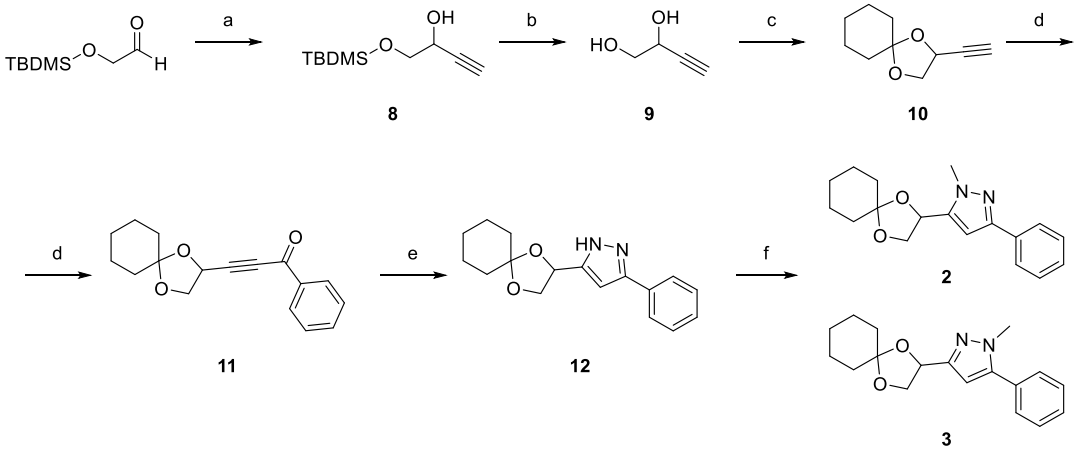

[a]Reagents and Conditions: (a) ethynylmagnesium bromide 0.5 M in THF (1.1 equiv), anh. THF, N_2 atmosphere, −15 °C, 15 min. (b) Amberlist-15 (100 mg per mmol), methanol, r.t., overnight, quantitative yield. (c) Cyclohexanone (1.1 equiv), pTSA (cat.), anh. toluene, N_2 atmosphere, reflux, Dean−Stark trap, 6 h, 49% yield. (d) Benzoyl chloride (1.5 equiv), $PdCl_2(PPh_3)_2$ (9% mol), CuI (3% mol), Et_3N (1.25 equiv), THF, rt, overnight. (e) Hydrazine (1.2 equiv), ethanol, r.t., overnight, 51% yield. (f) Dimethylsulfate (1 equiv), K_2CO_3 (2.5 equiv), DMF, 60 °C, overnight,, 52% yield (for **2**) and 40% yield (for **3**).

Scheme 2[a]

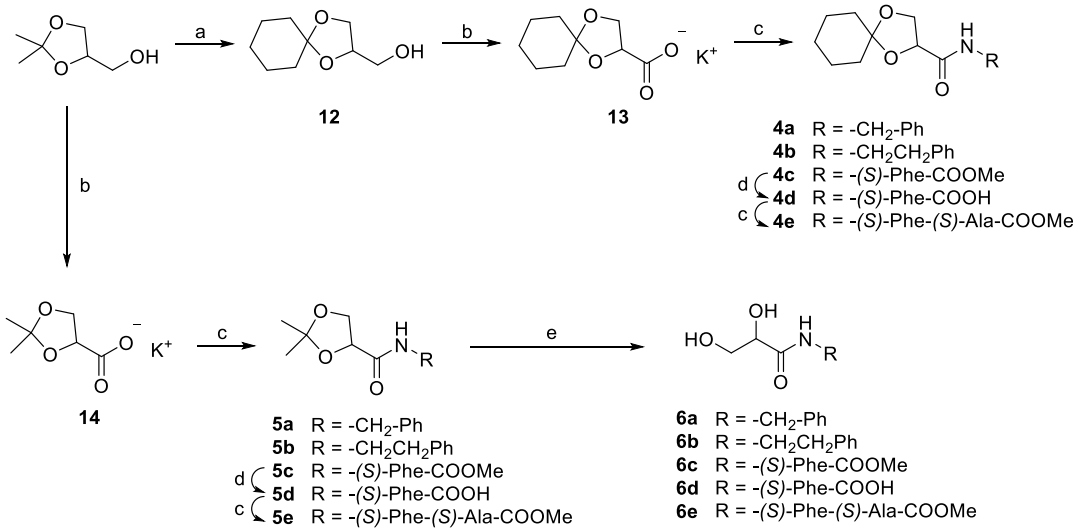

[a]Reagents and conditions: (a) cyclohexyl dimethyl ketal (1.2 equiv), Amberlyst-15 (100 mg per mmol), neat, 90 °C, 2 h, quantitative yield. (b) $KMnO_4$ (2.5 equiv), KOH (3 equiv), water, 0 °C to r.t., overnight. (c) Appropriate amine (1 equiv), EDC HCl (1 equiv), HOBt (0.1 equiv), TEA (1 equiv), anh. DMF, N_2 atmosphere, overnight, 66% yield (for **4a**), 64% yield (for **4b**), 57% yield (for **4c**), 56% yield (for **5a**), 63% yield (for **5b**), 68% yield (for **5c**). (d) 1 M aq LiOH (1.1 equiv), THF/methanol 3:1, r.t., 1 h, 91% yield (for **4d**), 95% yield (for **5d**). (e) pTSA (cat.), methanol/water 3:1, r.t., overnight, quantitative yield.

structure (**7a−e**). This modification also resulted in achiral derivatives on the aliphatic heterocyclic moiety, enabling the investigation of the role of chirality on antibiofilm activity. For a comprehensive SAR study, all functional modifications at the amidic moiety in the design of compounds **4a−e** were also retained in the new compounds derived from modifications in the dioxolane scaffold (**5a−e**, **6a−e**, and **7a−e**). Lastly, before addressing the designed molecules to synthesis, these were screened for pan-assay interference using the in silico tool FAFDrugs4, without revealing issues.[39]

Chemistry. The synthesis of pyrazole derivative **3** was carried out following previously reported methodologies, with minor modifications.[36] The synthesis process is outlined in Scheme 1. Initially, (*tert*-butyldimethylsilyloxy) acetaldehyde was converted into the secondary alcohol **8** by reacting with ethynylmagnesium bromide in anhydrous THF at −15 °C, under a nitrogen atmosphere for 15 min. Subsequent deprotection of the silyl-protected hydroxyl group to yield the corresponding diol **9** was accomplished using a sulfonic resin (Amberlist-15) as acid catalyst in methanol under gentle shaking overnight. The use of this resin enabled the attainment of diol **9** in high yield and purity simply by filtering the methanolic solution from the resin and then concentrating it. This approach obviated the need for an acid solution and the subsequent organic/basic aqueous solution liquid−liquid workup procedure, thus preventing the loss of product **9** in the aqueous phase due to its high hydrophilicity. Diol **9** was protected as a cyclohexylspirodioxolane through reaction with

https://doi.org/10.1021/acs.jmedchem.4c01266
J. Med. Chem. 2024, 67, 18139−18156

Scheme 3[a]

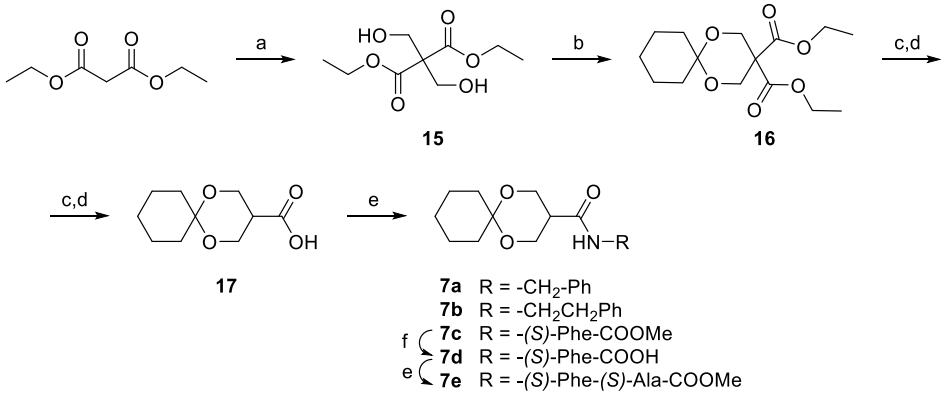

[a]Reagents and conditions: (a) 30% w/v aq formaldehyde (3 equiv), $NaHCO_3$ (0.1 equiv), neat, r.t., 90% yield. (b) Cyclohexanone (1.1 equiv), pTSA (cat.), anh. toluene, N_2 atmosphere, reflux, Dean−Stark trap, 2 h, 37% yield; (c) KOH (3 equiv), THF/EtOH 3:1, r.t., overnight. (d) Pyridine, reflux, N_2 stream, 3 h, 70% yield. (e) Appropriate amine (1 equiv), EDC HCl (1 equiv), HOBt (0.1 equiv), TEA (1 equiv), anh. DMF, N_2 atmosphere, overnight, 48% yield (for **7a**), 52% yield (for **7b**), 71% yield (for **7c**), 83% yield (for **7e**). (f) 1 M aq LiOH (1.1 equiv), THF/methanol 3:1, r.t., 1 h, 95% yield.

cyclohexanone and a catalytic amount of *p*-toluenesulfonic acid (pTSA). The condensation was performed in refluxing toluene under a Dean−Stark trap to remove the water formed during the reaction. The Sonogashira coupling of the terminal alkyne **10** with benzoyl chloride to achieve the propyn-1-one **11** was then performed using $PdCl_2(PPh_3)_2$ and CuI as catalysts and triethylamine (TEA) as base in THF at room temperature overnight. Lastly, the cyclization of compound **11** to the target pyrazole **1** was performed using hydrazine in ethanol.[40] The methylation of **1** by reaction with dimethyl sulfate in dimethylformamide (DMF), using potassium carbonate (K_2CO_3) as the base, produced both isomers **2** and **3**. The two isomers were easily separated and purified by column chromatography (Scheme 1).

The synthesis of the cyclohexyl spirodioxolane derivatives **4a−e**, as well as the ketal-derivatives **5a−e**, and diol-derivatives **6a−e** is comprehensively delineated in Scheme 2. The synthesis started with the transformation of solketal into the spiro alcohol **12**.[41] This was achieved by reacting solketal with cyclohexyl dimethyl ketal in the presence of Amberlyst-15 (100 mg per mmol) at 90 °C. The reaction was driven toward completion by distillation of the forming acetone, effectively shifting the *trans*-ketalization equilibrium toward the desired product. Subsequently, alcohol **12** underwent oxidation to yield the potassium carboxylate salt **13**. This step was performed using an aqueous alkaline potassium permanganate solution at room temperature, overnight. The derivatives **4a−c** were synthesized through a direct reaction of compound **13** with various amines. Specifically, benzylamine was used for **4a**, 2-phenylethylamine was used for **4b**, and L-phenylalanine methyl ester was used for **4c**. The reaction was performed in standard coupling conditions using 1-ethyl-3-(3-(dimethylamino)propyl)carbodiimide (EDC) and hydroxybenzotriazole (HOBt) as coupling agents, conducted in DMF from 0 °C to room temperature overnight. The compound **4c** was hydrolyzed to yield the carboxylic acid **4d** using a 1 M aqueous solution of LiOH in a THF/MeOH mixture (3:1 v/v ratio), at room temperature for 1 h. The choice of LiOH for ester hydrolysis was critical to prevent racemization at the α-carbon of phenylalanine. The final derivative, **4e**, was obtained by reacting **4d** with L-alanine methyl ester under standard coupling conditions. For the synthesis of the ketal derivatives **5a−e**, the same synthetic scheme and procedures used for **4a−e** were employed but utilizing the potassium carboxylate **14**. This carboxylate was prepared through the oxidation of solketal, following a similar methodology to that described for the synthesis of the cyclohexyl spirodioxolane derivatives **12**. The final series of derivatives, **6a−e**, were synthesized from the corresponding ketal-derivatives **5a−e**. This process involved the hydrolysis of the dimethyl ketals, which was efficiently carried out in a methanol/water mixture with a ratio of 3:1. For this hydrolysis reaction, a catalytic amount of pTSA was utilized. The use of pTSA as a catalyst facilitated the hydrolysis under mild conditions, ensuring the efficient conversion of the ketal-derivatives **5a−e** to their respective hydrolyzed products **6a−e** without any significant side reactions or degradation of the products (Scheme 2).

The synthesis of compounds **7a−e** followed a similar synthetic scheme and procedures as those utilized to prepare derivatives **4a−e** and **5a−e**, with the initial precursor being cyclohexyl spiro-1,3-dioxane carboxylic acid (**17**). As reported in Scheme 3, the synthesis of this key intermediate was performed as previously reported.[42] In the first step, diethyl malonate was reacted with aqueous formaldehyde, leading to the formation of diol **15**. This step involved a condensation reaction, where the aldehyde group of formaldehyde reacted with the alpha-carbon of diethyl malonate, forming a new diol moiety. **15** was further condensed with cyclohexanone in the presence of a catalytic amount of pTSA. This reaction was like the previously mentioned ketalization steps, resulting in the formation of the bis-diethyl ester compound **16**. Both ester moieties in compound **16** were hydrolyzed using aqueous KOH. The achieved bis-carboxylic acid was directly subjected to decarboxylation under refluxing conditions in pyridine, and a nitrogen stream. This step removed one carboxyl group, resulting in the formation of compound **17**. Once compound **17** was synthesized, it served as the starting point for the preparation of derivatives **7a−e**, utilizing the established synthetic procedures like those used for the synthesis of the previously mentioned derivatives (Scheme 3).

Following the synthetic route outlined in Scheme 2, homochiral compounds (5*S*,11*S*)-**5d**, (5*R*,11*S*)-**5d**, and (5*S*,11*S*,22*S*)-**5e**, and (5*R*,11*S*,22*S*)-**5e** were synthesized

https://doi.org/10.1021/acs.jmedchem.4c01266
J. Med. Chem. 2024, 67, 18139−18156

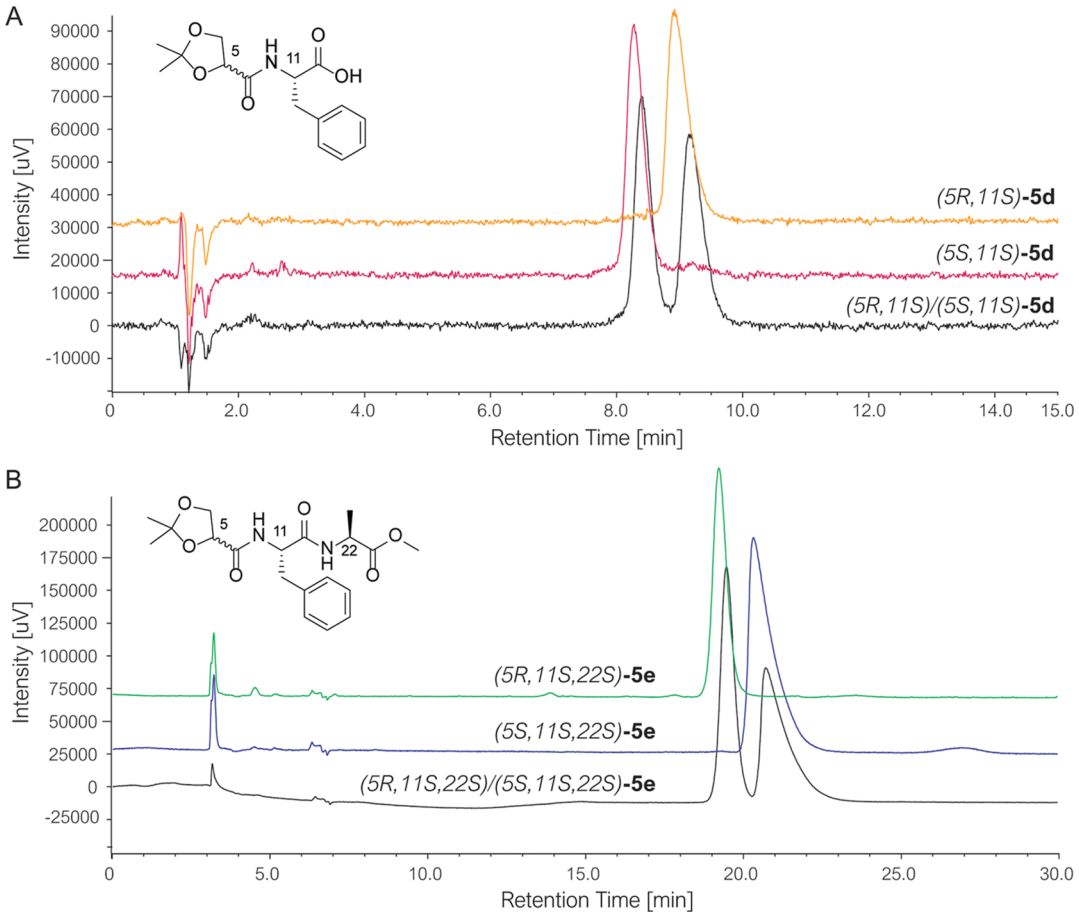

Figure 4. (A) UV/vis-HPLC trace (λ = 220 nm) for compounds **5d**, (5*S*,11*S*)-**5d** and (5*R*,11*S*)-**5d** on symmetry C-18 (3.9 × 150 mm, 5 μm), eluent water/methanol/formic acid 50:50:0.1 (v/v/v), flow rate: 1 mL/min, T = 25 °C, an injection volume of 10 μL, a concentration of 1 mg/mL. (B) UV/vis-HPLC trace (λ = 220 nm) for compounds **5e**, (5*S*,11*S*,22*S*)-**5e** and (5*R*,11*S*,22*S*)-**5e** on Chiralpak IA (4.6 × 250 mm, 5 μm), eluent hexane/isopropanol 90:10 (v/v/v), flow rate: 1 mL/min, T = 25 °C, an injection volume of 10 μL, a concentration of 1 mg/mL.

starting from the commercially available enantiomerically pure (*S*)-methyl 2,2-dimethyl-1,3-dioxolane-4-carboxylate and (*R*)-methyl 2,2-dimethyl-1,3-dioxolane-4-carboxylate, respectively. Homochiral methyl 2,2-dimethyl-1,3-dioxolane-4-carboxylate was hydrolyzed to the corresponding carboxylic acid (*S*)-**14** and (*R*)-**14**, using aqueous LiOH in THF/MeOH 3:1 at room temperature for 1 h, without observing racemization or partial inversion of the configuration on the stereogenic carbon of the dioxolane moiety. The coupling of (*S*)-**14** and (*R*)-**14** with L-phenylalanine methyl ester, using EDC and HOBt as coupling reagents, gave (5*S*,11*S*)-**5c** and (5*R*,11*S*)-**5c**, respectively. Subsequent hydrolysis using aqueous LiOH, followed by crystallization from water, yielded the corresponding diastereomers (5*S*,11*S*)-**5d** and (5*R*,11*S*)-**5d**. Both diastereomers were further reacted with L-alanine methyl ester under standard coupling conditions as described above to afford (5*S*,11*S*,22*S*)-**5e** and (5*R*,11*S*,22*S*)-**5e**, respectively, as confirmed by NMR. Specifically, the correct pairs of equivalent but stereochemical distinct ^{1}H NMR signals from diastereotopic methylene groups—each corresponding to one of the two diastereomers—were selected for integration to calculate the diastereomeric ratio. We focused particularly on the diastereotopic methylene protons of the dioxolane moiety in α position to the amide, which produced two distinct and nonoverlapping double doublets at δ 3.92 and 4.05 ppm for (5*S*,11*S*)-**5d** and (5*R*,11*S*)-**5d** (Figure S1) and at δ 3.79 and 4.05 ppm for (5*S*,11*S*,22*S*)-**5e** and (5*R*,11*S*,22*S*)-**5e** (Figure S2), respectively. Additionally, for **5e,** the methyl ester group of the alanine moiety generated distinct singlets at 3.66 and 3.64 ppm for the two diastereomers. All other signals in the diastereomeric mixture overlapped and were thus unsuitable for calculating diastereomeric ratios.

The diastereomeric excess of (5*S*,11*S*)-**5d**, (5*R*,11*S*)-**5d**, (5*S*,11*S*,22*S*)-**5e,** and (5*R*,11*S*,22*S*)-**5e** was determined by HPLC. To set up the HPLC analytical method, **5d** and **5e** were used since they were initially synthesized as a diastereomeric mixture, starting from racemic **14**. For (5*S*,11*S*)-**5d**, (5*R*,11*S*)-**5d** baseline separation was achieved on a symmetry C-18 (3.9 × 150 mm, 5 μm), under isocratic elution conditions with a mobile phase composed of water, methanol, and formic acid in a 50:50:0.1 (v/v/v) ratio (Figure 4A), whereas for (5*S*,11*S*,22*S*)-**5e** and (5*R*,11*S*,22*S*)-**5e**, no baseline separation was achieved on the nonchiral reverse stationary phase using different mobile phase compositions (data not shown). Therefore, a different approach was attempted, evaluating an enantioselective HPLC separation method. They were successfully separated on a Chiralpak IA (4.6 × 250 mm, 5 μm) under isocratic elution conditions with a mobile phase composed of hexane and isopropanol in a 90:10 (v/v) ratio (Figure 4B). The analysis revealed that both diastereomers (5*S*,11*S*)-**5d** and (5*R*,11*S*)-**5d** and

https://doi.org/10.1021/acs.jmedchem.4c01266
J. Med. Chem. 2024, 67, 18139−18156

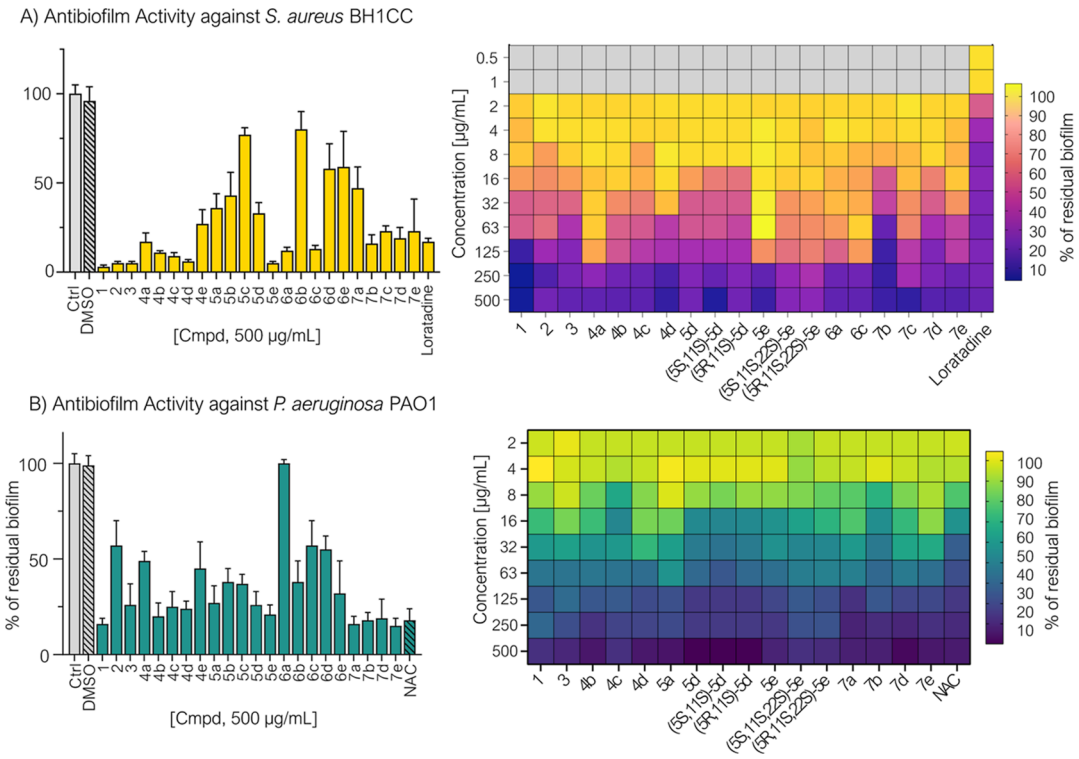

Figure 5. Biofilm inhibition activity for compounds **1**−**3**, **4a**−**e**, **5a**−**e**, **6a**−**e**, **7a**−**e**, NAC, and loratadine at 500 μg/mL (left) and in dose−response assay for the determination of the $MBIC_{50}$ (right) in *S. aureus* (A) and *P. aeruginosa* (B). Biofilms were grown in sterile 96-well polystyrene plates in BHI (A) or LB medium (B), supplemented with glucose, for 24 h at 37 °C. After washing, cells were stained with crystal violet, and the absorbance was measured at 595 nm. Biofilm levels are expressed as a percentage compared to controls, where biofilm was grown in the absence of potential inhibitors. Control with DMSO alone was conducted to exclude effects of the organic solvent on biofilm formation. Data are representative of three independent experiments and are expressed as means ± STD.

(5*S*,11*S*,22*S*)-**5e** and (5*R*,11*S*,22*S*)-**5e** were obtained with a diastereomeric excess >99%.

Evaluation of the Antibiofilm Activity on *P. aeruginosa* PAO1 and *S. aureus* BH1CC Strains. All of the newly synthesized compounds (**3**, **4a**−**e**, **5a**−**e**, **6a**−**e**, and **7a**−**e**) together with compounds **1** and **2** were initially assessed to evaluate their capacity to affect biofilm formation using a crystal violet staining assay, which quantifies biofilm biomass. To enhance the relevance of the current study in solving the infection problem, we used the bacterial model *P. aeruginosa* PAO1 and *S. aureus* BH1CC. All the compounds were initially tested at a fixed concentration of 500 μg/mL. The residual biofilm formation was determined after 24 h from exposure of the bacterial culture to compounds under investigation. *N*-Acetylcysteine (NAC) and loratadine, two drugs well-characterized for their capability to interfere with biofilm formation by *P. aeruginosa* and *S. aureus*, respectively, were used as reference compounds.[43]

The results of the assay are reported in Figure 5 and Table S1 and are expressed as a percentage of residual biofilm formation compared to the control (no compounds added). The best hits for antibiofilm activity against at least one bacterial strain were prioritized for secondary assay. A cutoff of 25% in residual biofilm formation at 500 μg/mL was set for picking out the most active compounds that were therefore tested in dose−response studies (from 500 to 2 μg/mL) for the determination of the $MBIC_{50}$, the concentration of compound required to inhibit 50% of biofilm formation (Table 1). NAC and loratadine exhibited an $MBIC_{50}$ of 14 and 2.5 μg/mL, comparable with the value reported in literature.[44−46]

In the evaluation of the $MBIC_{50}$ data against both *S. aureus* and *P. aeruginosa* biofilm formation, a span of inhibitory biofilm formation concentrations could be observed. The study identified various compound subsets displaying selective or dual biofilm inhibitory effectiveness against these bacterial strains. Specifically for *S. aureus*, compounds **7b**, **7d**, and **5d** emerged as the most effective biofilm inhibitors, exhibiting low $MBIC_{50}$ values at 16.9, 20.6, and 34.6 μg/mL, respectively. This was followed by compounds **1**−**3**, **4a**−**d**, **5d**−**e**, **6c**, **7c**, and **7e**, demonstrating moderate inhibitory potential ($MBIC_{50}$ ranging from 16.2 to 191.3 μg/mL). In contrast, compounds **4e**, **5b**, **5c**, and **6b** exhibited limited or no antibiofilm activity in the primary assay. Focusing on *P. aeruginosa*, most tested compounds in dose−response studies showed effective biofilm formation inhibition with $MBIC_{50}$ < 60.5 μg/mL. Conversely compounds **2**, **4a**, **4e**, **5b**, **5c**, **6a**−**e**, and **7c** demonstrated limited or no antibiofilm efficacy in the primary assay, with estimated $cMBIC_{50}$ values over 500 μg/mL. It is particularly notable that compounds **5d** and **5e** exhibited $MBIC_{50}$ values of 27.7 and 29.1 μg/mL respectively, and that **7b** resulted in the most potent compound in the entire library with a $MBIC_{50}$ value of 6.2 μg/mL. Following promising MBIC results of **5d** and **5e** against both *S. aureus* and/or *P. aeruginosa*, the role of chirality was investigated by preparing and evaluating diasteropure (5*S*,11*S*)-**5d**, (5*R*,11*S*)-**5d**, (5*S*,11*S*,22*S*)-**5e**, and (5*R*,11*S*,22*S*)-**5e**. As detailed in Table 1, both diastereomers of compounds **5d** exhibit comparable antibiofilm activities against *S. aureus* $MBIC_{50}$ of 26.3 and 25.4 μg/mL for (5*S*,11*S*)-**5d**,

https://doi.org/10.1021/acs.jmedchem.4c01266
J. Med. Chem. 2024, 67, 18139−18156

Table 1. Biofilm Inhibition Activity for Compounds 1−3, 4a−e, 5a−e, 6a−e, and 7a−e and Diastereomers (5*S*,11*S*)-5d, (5*R*,11*S*)-5d, (5*S*,11*S*,22*S*)-5e, (5*R*,11*S*,22*S*)-5e in *S. aureus* and *P. aeruginosa*[a,b]

cmpd	*S. aureus* $MBIC_{50}$ in μg/mL	*P. aeruginosa* $MBIC_{50}$ in μg/mL
1	45.1 ± 7.4	22.5 ± 3.2
2	55.2 ± 10.1	N/D
3	121.4 ± 19.1	37.3 ± 11.1
4a	191.3 ± 16.0	N/D
4b	92.3 ± 12.1	38.3 ± 11.0
4c	71.1 ± 13.2	60.5 ± 5.2
4d	61.5 ± 11.3	46.2 ± 7.5
5a	N/D	36.6 ± 9.0
5d	34.6 ± 6.9	27.7 ± 5.7
(5*S*,11*S*)-**5d**	26.3 ± 5.1	34.4 ± 5.3
(5*R*,11*S*)-**5d**	25.4 ± 4.6	30.4 ± 5.0
5e	152.3 ± 18.3	29.1 ± 4.1
(5*S*,11*S*,22*S*)-**5e**	82.2 ± 30.5	25.4 ± 9.6
(5*R*,11*S*,22*S*)-**5e**	169.7 ± 28.3	31.7 ± 12.4
6a	128.2 ± 16.9	N/D
6c	173.0 ± 25.3	N/D
7a	N/D	40.8 ± 10.7
7b	16.2 ± 8.1	6.2 ± 3.6
7c	85.8 ± 18.5	N/D
7d	20.6 ± 4.4	50.0 ± 9.1
7e	55.9 ± 13.9	48.3 ± 4.8
NAC	N/D	14 ± 3.3
loratadine	2.5 ± 1.8	N/D

[a]Data are representative of three independent experiments and are expressed as means ± STD. N/D: not determined. [b]For compounds that showed a percentage of residual biofilm <25% at 500 μg/mL, the $MBIC_{50}$ (in μg/mL) was determined in dose−response studies.

(5*R*,11*S*)-**5d**. Conversely, diastereoisomer (5*S*,11*S*,22*S*)-**5e** resulted twice more active than (5*R*,11*S*,22*S*)-**5e** with an $MBIC_{50}$ of 82.2 and 169.7 μg/mL, respectively. Instead, no diastereoselectivity was observed in the capacity of compounds **5d** and **5e** to disrupt biofilm formation by *P. aeruginosa* ($MBIC_{50}$ values of 34.4 and 30.4 μg/mL for (5*S*,11*S*)-**5d**, (5*R*,11*S*)-**5d** and 25.4 and 31.7 μg/mL for (5*S*,11*S*,22*S*)-**5e**, and (5*R*,11*S*,22*S*)-**5e**). These results suggest that the stereochemical configuration at the dioxolane moiety does not significantly impact of the antibiofilm efficacy of these compounds.

Effect on Bacterial Growth. QSIs differ from antibiotics in their mechanisms of action. Unlike antibiotics, which kill pathogenic bacteria, QSIs inhibit the production of virulence factors and biofilm formation without affecting bacteria vitality. Therefore, to evaluate whether the antibiofilm activity of the tested compounds is mediated through QS inhibition rather than direct antimicrobial action, we tested the effect of the most active compounds in inhibiting biofilm formation (**1**, **3**, **4d**, **5d−e**, and **7b**) on both *P. aeruginosa* and *S. aureus* bacterial growth. Bacterial cultures were incubated with 500 μg/mL of the tested compounds, and cell growth was monitored spectrophotometrically by measuring the absorbance of the cell cultures at 600 nm for 20 h. The results demonstrate that none of the tested compounds adversely affected bacterial growth, thus confirming an QS-mediated antibiofilm activity (Figures S3 and S4).

Inhibition of AI-2 Mediated QS Activity on *Vibrio harveyi* by Compounds 5d, 5e, and 7b. The QS inhibitor activity of the most potent compounds, which demonstrated significant inhibition of biofilm formation in *S. aureus* and *P. aeruginosa* (**5d**, **5e**, and **7b**), was evaluated through cellular assays using genetically engineered *V. harveyi* strains. These assays were designed to highlight the inhibitor potential of the molecules to interfere with QS mechanisms. *V. harveyi* BB170 (BAA-1117, ATCC), sis a mutant strain designed to respond exclusively to AI-2, facilitating bioluminescence, and it was utilized to assess the capability of compounds **5d**, **5e**, and **7b** to specifically inhibit AI-2 mediated QS. Since diastereomers **5d** and **5e** did not show any differences in antibiofilm activity, they have been evaluated as diastereomeric mixtures. Additionally, the QS inhibitory activity of the compounds was tested on *V. harveyi* BB120 (BAA-1116, ATCC) and BB886 (BAA-1118, ATCC) strains, serving as positive and negative controls, respectively. BB120, a wild-type strain, responds to both AI-1 and AI-2 signals, while BB886, a mutant strain, is responsive solely to AI-1 autoinducers. Before proceeding with the QSI assays, concentrations ranging from 4 to 500 μg/mL of each compound were evaluated for their impact on bacterial growth, with none showing an effect on growth rates (data not shown). Compound Str7410 was reported by Jiang et al. as an effective *V. harveyi* BB170 AI-2 mediated QSI with an IC_{50} of 0.4 μM. It was synthesized by us according to the protocol published, and it was used as a positive control.[47] To assess AI-2 inhibition, the bacterial strains were incubated in cell-free supernatant (CFS) derived from each overnight culture, enriched with AI-2 and/or AI-1 autoinducer levels produced during overnight growth. This was done to induce luminescence in the presence of the compounds at a concentration of 500 μg/mL. Reduction in the luminescence level after 8 h of incubation with the compounds compared with the corresponding control (bioluminescence of cells diluted and incubated in CFS in the absence of compounds) was indicative of a QS quenching. AI-2 signaling activity is reported as the percentage of bioluminescence for each sample relative to its control. The positive control Str7410 was tested at its IC_{50}, and the results are in accordance with the literature.[45] As reported in Figure 6, all three tested compounds demonstrated significant QS inhibitory activity in both BB120 and BB170 strains. The addition of compounds **5d**, **5e**, and **7b** led to a marked reduction in bioluminescence, confirming their role as QS inhibitors of AI-2 activity. Conversely, no inhibition was detected by any tested

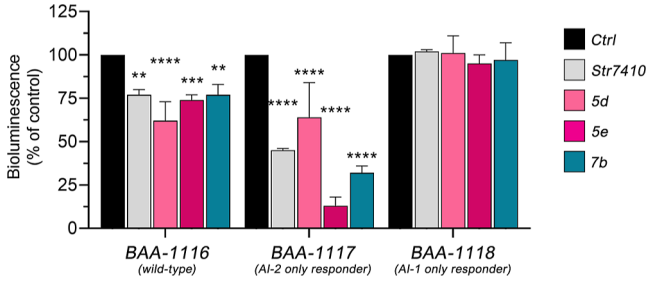

Figure 6. Anti-*Vibrio harveyi* QS activities of tested compounds. Bacterial cells were incubated in CFS in the presence or absence of compounds for 8 h at 30 °C under shaking (100 rpm). Bioluminescence ($OD_{460\ nm}$) was normalized over cell density ($OD_{600\ nm}$). Bioluminescence levels of bacteria incubated with each compound were expressed as % of control (no compound added). One-way Anova test was used to perform statistical analysis: vs ctrl $^{**}p < 0.1$; $^{***}p < 0.01$; $^{****}p < 0.001$.

https://doi.org/10.1021/acs.jmedchem.4c01266
J. Med. Chem. 2024, 67, 18139−18156

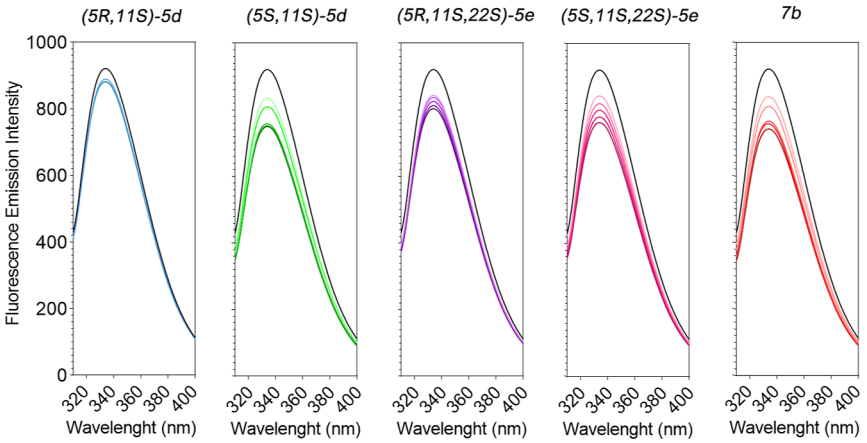

Figure 7. Fluorescence quenching spectra of LsrK in the presence of (5*R*,11*S*)-**5d**, (5*S*,11*S*)-**5d**, (5*S*,11*S*,22*S*)-**5e**, (5*R*,11*S*,22*S*)-**5e**, and **7b**, [LsrK] = 1.0 μM, [ligand] ranging from 31.25 to 500 μM, T = 298 K, pH = 7.4, λ_{ex} = 295 nm; the experiments are performed in duplicate.

compound on the AI-1 responsive BB886 strain (Figure 6). This outcome confirms the specificity of our compounds for AI-2-mediated activities.

Evaluation of the Ligand−LsrK Binding through Spectroscopic-Based Biophysical Approaches. Upon establishing that the compounds under investigation (i) inhibit biofilm formation in *S. aureus* and *P. aeruginosa* strains, (ii) do not affect the growth and viability of bacteria in their planktonic forms, (iii) inhibit AI-2-mediated QS, and (iv) were designed as structural analogues of AI-2, their ability to interact with LsrK was examined. To this end, two fluorescence-based techniques (e.g., DSF and ITF) and CD were employed as biophysical techniques.

DSF Assay. DSF is a widely recognized method for rapidly evaluating protein−ligand interactions. This technique is based on the principle that proteins denature and unfold upon thermal heating, thereby exposing internal hydrophobic surfaces.[48] These surfaces bind to SYPRO Orange dye, leading to an increased fluorescence signal due to the exclusion of water. The binding of small molecules can modify the protein's thermal stability, manifesting as a shift in the melting temperature (T_m).[49] Compounds (5*S*,11*S*)-**5d**, (5*R*,11*S*)-**5d**, (5*S*,11*S*,22*S*)-**5e**, (5*R*,11*S*,22*S*)-**5e**, and **7b** were screened at a concentration of 500 μg/mL. Additionally, ATP and (*S*)-DPD, the natural substrates of LsrK, were evaluated as reference compounds. ATP, which has a Michaelis−Menten constant (K_m) of 130 μM for LsrK, induced a change in T_m (ΔT_m) of 1.0 °C at a concentration of 1.0 mM, which is 8-fold higher than its K_m. In contrast, (*S*)-DPD did not exhibit a thermal shift when tested independently, aligning with the kinetic mechanism of LsrK which necessitates ATP binding before substrate recognition.[50] For assessing compound efficacy, a threshold of ΔT_m > 1.0 °C was established based on result of ATP, serving as the criterion for a positive thermal shift. All five compounds demonstrated thermal shift values exceeding ΔT_m > 1.0 °C at 500 μg/mL, indicating their potential to stabilize LsrK similarly to its natural substrate. Furthermore, considering that LsrK has two distinct binding sites, one for ATP and another for DPD, investigations were extended to determine the probable binding site of the new compounds by assessing them in combination with an equimolar concentration of ATP. Co-treatment with ATP and compounds **5d**, **5e**, and **7b** resulted in a ΔT_m > 2.0 °C. This additive effect suggests that the DPD-derived compounds likely do not compete with ATP for the same binding site, indicating distinct sites of action.

Intrinsic Tryptophan Fluorescence Spectroscopy Assay. To support the ligand−protein interactions observed through DSF, we employed intrinsic tryptophan fluorescence spectroscopy (ITF) as a complementary technique.[51] The LsrK enzyme, characterized by a high tryptophan content with 13 residues highly conserved across different bacterial species, proved ideal for this study. Consequently, variations in the intrinsic fluorescence of Trp residues, in response to protein titration with the ligand, suggest ligand-induced changes within the protein. In our earlier research, we introduced and validated ITF as an effective and straightforward analytical technique to identify promising candidates that bind LsrK.[51] Measurements were conducted by exciting the protein at a wavelength of 295 nm and collecting the emission spectrum in the 310−400 nm range. The intrinsic fluorescence of LsrK at 1 μM in saline phosphate-buffered is reported in Figure 7, showing an emission peak at 330 nm, typical of proteins with tryptophan residues both exposed to solvent and internal. The fluorescence emission spectra recorded in the range 310−400 nm in the presence of increasing concentrations of compounds (5*S*,11*S*)-**5d**, (5*R*,11*S*)-**5d**, (5*S*,11*S*,22*S*)-**5e**, (5*R*,11*S*,22*S*)-**5e**, and **7b** are reported in Figure 7. The analysis revealed that all tested compounds induce a dose-dependent decrease in the fluorescence intensity of LsrK, suggesting binding with the enzyme. Additionally, tryptophan fluorescence spectroscopy offered the opportunity to explore the interaction differences between the two diastereomers of compound **5d**. The collected data indicate a slight binding preference with diastereomer (5*S*,11*S*)-**5d** exhibiting a higher capability to induce an LsrK fluorescence quenching compared to its isomer (5*R*,11*S*)-**5d** as highlighted by the maximum reduction in fluorescence intensity, which resulted in 12% and 6% for (5*S*,11*S*)-**5d** and (5*R*,11*S*)-**5d**, respectively.

CD Assay. To confirm the results obtained from both fluorescence spectroscopy techniques, CD was used as an orthogonal assay. In our previous work, we assessed the reliability of CD to assess the binding of some secondary metabolites with LsrK. Indeed, CD is a quantitative and sensitive technique used to study the protein conformation and changes in the secondary structure of protein upon interaction with a ligand molecule. The structural changes of LsrK and the efficiency of binding of LsrK with compounds (5*R*,11*S*)-**5d**,

https://doi.org/10.1021/acs.jmedchem.4c01266
J. Med. Chem. 2024, 67, 18139−18156

(5*S*,11*S*)-**5d**, and **7b** were studied using CD spectra. Conversely, for compounds (5*S*,11*S*,22*S*)-**5e** and (5*R*,11*S*,22*S*)-**5e**, the high UV absorbance at wavelength <220 nm prevented a reliable interpretation of the induced CD spectra (Figures S6 and S7). Accordingly, CD spectra of LsrK alone and in the presence of the tested compounds at ligand/LsrK molar ratio of 1:1 and 10:1 were recorded to decipher the structural and conformational changes in the secondary structure of the protein. CD spectra of LsrK in the absence and presence of the tested compounds are shown in Figure 8. Since compounds (5*R*,11*S*)-**5d** and (5*S*,11*S*)-**5d** are

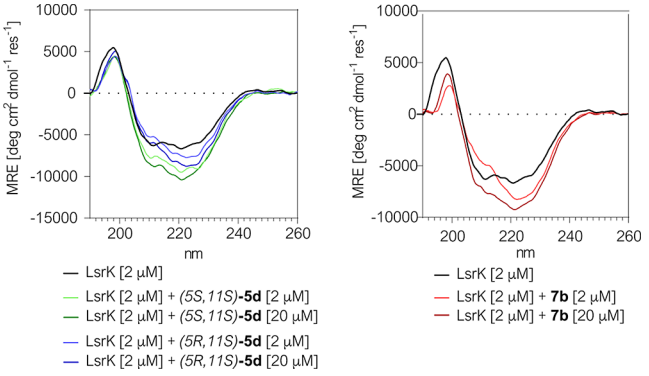

Figure 8. Far-UV CD spectra of LsrK in the presence or absence of the indicated compounds. The reported spectra are the average of six scans and corrected for CD spectra of the sole compound.

optically active compounds, their CD spectra were recorded under the same conditions and used to correct the ligand−protein-induced CD spectra. Far UV-CD spectra of apo-LsrK at 2 μM revealed a positive band at 195 nm and a negative band with two characteristic negative bands at 208 and 222 nm, attributed to n → π^* and $\pi \rightarrow \pi^*$ transitions of the α-helical structure. Deconvolution of the CD spectrum using BestSel[52] confirmed that the protein is a mainly helix-strand protein and allowed us to estimate the relative content of the secondary structure elements of the protein (rmsd 0.3828) (Table S2). This result agrees with the crystallographic structure of the protein and the secondary structure content calculated from the available crystallographic structure of the apo-LsrK (PDB ID: 5YA0), thus confirming the stability and the proper native folding of the enzyme in the CD experimental conditions. Any alteration in these bands in the presence of a compound would indicate the structural variations in the LsrK. As can be seen from Figure 8, adding compounds (5*R*,11*S*)-**5d**, (5*S*,11*S*)-**5d**, and **7b** decreases the ellipticity at 200, 208, and 222 nm in a dose-dependent manner. This suggests a shift of LsrK toward a more orderly conformation because of the interaction of the protein with ligands. Therefore, CD analysis showed that the interaction of the identified compounds with LsrK clearly leads to protein conformational changes, thus confirming their ability to interact with the enzyme.

Overall, these three distinct and complementary biophysical techniques have collectively provided robust evidence supporting the effective interaction of test compounds **5d**, **5e**, and **7b** with the LsrK protein.

NMR Interaction Studies and Binding Epitope Mapping. NMR is a versatile and sensitive method to detect binding. A combination of ligand-based NMR approaches, namely, ^{1}H line-broadening experiments[37,38] and STD experiments[53] confirmed the binding of (5*S*,11*S*)-**5d**, (5*S*,11*S*,22*S*)-**5e**, and **7b** to LsrK. NMR studies demonstrated a tighter binding of the **7b** compound to LsrK with respect to (5*S*,11*S*)-**5d** and (5*S*,11*S*,22*S*)-**5e**. A K_D in the low micromolar range could be inferred for **7b** from the significant line broadening of resonances in the presence of the protein (Figure S8). In line with this observation, negligible STD NMR effects were observed for **7b**. Measurable STD effects were observed for (5*S*,11*S*)-**5d** and (5*S*,11*S*,22*S*)-**5e** allowing for the characterization of their binding epitopes and suggesting a higher K_D for the two compounds with respect to **7b** (Figure 9). Series of STD NMR experiments at different saturation times were carried out to monitor the growth of saturation transfer (Figure S9) and gain molecular information about the binding epitopes. The initial growth rates (STD_0) were derived as described in Material and Methods (Tables S3 and S4) and mapped on the molecules to highlight ligand protons which are the nearest to the protein (Figure 9).[54]

The binding epitope mappings derived for (5*S*,11*S*)-**5d** and (5*S*,11*S*,22*S*)-**5e** showed very high normalized STD values, above 90%, for the phenyl group protons, demonstrating that both molecules establish very close contacts with LsrK through the aromatic moiety. A lower contribution to the recognition came from the methyls of the (5*S*,11*S*,22*S*)-**5e** alanine and methoxy group, as deduced from normalized STD values <75%.

These studies are crucial in elucidating the mechanistic details of how these structural analogues of AI-2 engage with LsrK, offering significant insights into their potential to modulate the AI-2 mediated QS pathway.

CONCLUSIONS

In conclusion, in the present study, we significantly advanced our development of novel anti AI-2 QSIs with antibiofilm activities against both Gram-positive and Gram-negative bacteria. By systematically exploring the chemical space around the DPD-based derivatives, we identified several compounds with promising inhibitory effects on biofilm formation, particularly against *S. aureus* and *P. aeruginosa*. Notably, compounds **5d**, **5e**, and **7b** exhibited notable inhibitory activity with a remarkably low $MBIC_{50}$, against both bacterial strains. The in-depth biological evaluation confirmed that the antibiofilm activities of our compounds are predominantly mediated through QS inhibition rather than direct antimicrobial effects. This mode of action was attested by the lack of significant growth inhibition in bacterial cultures treated with our lead compounds and by the capability of the tested compounds to selectively quench the AI-2 mediated QS in a cellular assay on engineered *V. harveyi* strains. Furthermore, the exploitation of advanced spectroscopic techniques to assess the ligand−LsrK interactions has provided deep insights into the mechanism underpinnings of QS inhibition. The DSF, ITF, CD and NMR studies have collectively confirmed the successful binding of our potent compounds to the LsrK enzyme, crucial for AI-2 mediated QS in bacteria. The atomic level details of (5*S*,11*S*)-**5d** and (5*S*,11*S*,22*S*)-**5e** interaction with LsrK, provided by STD NMR spectroscopy, highlighted the primary role of inhibitor phenyl group in protein recognition. Overall, these findings not only enhance our understanding of QS modulation through small molecule inhibitors but also pave the way for developing novel therapeutic strategies against biofilm-associated infections and AMR. The compounds identified and evaluated in our

https://doi.org/10.1021/acs.jmedchem.4c01266
J. Med. Chem. 2024, 67, 18139−18156

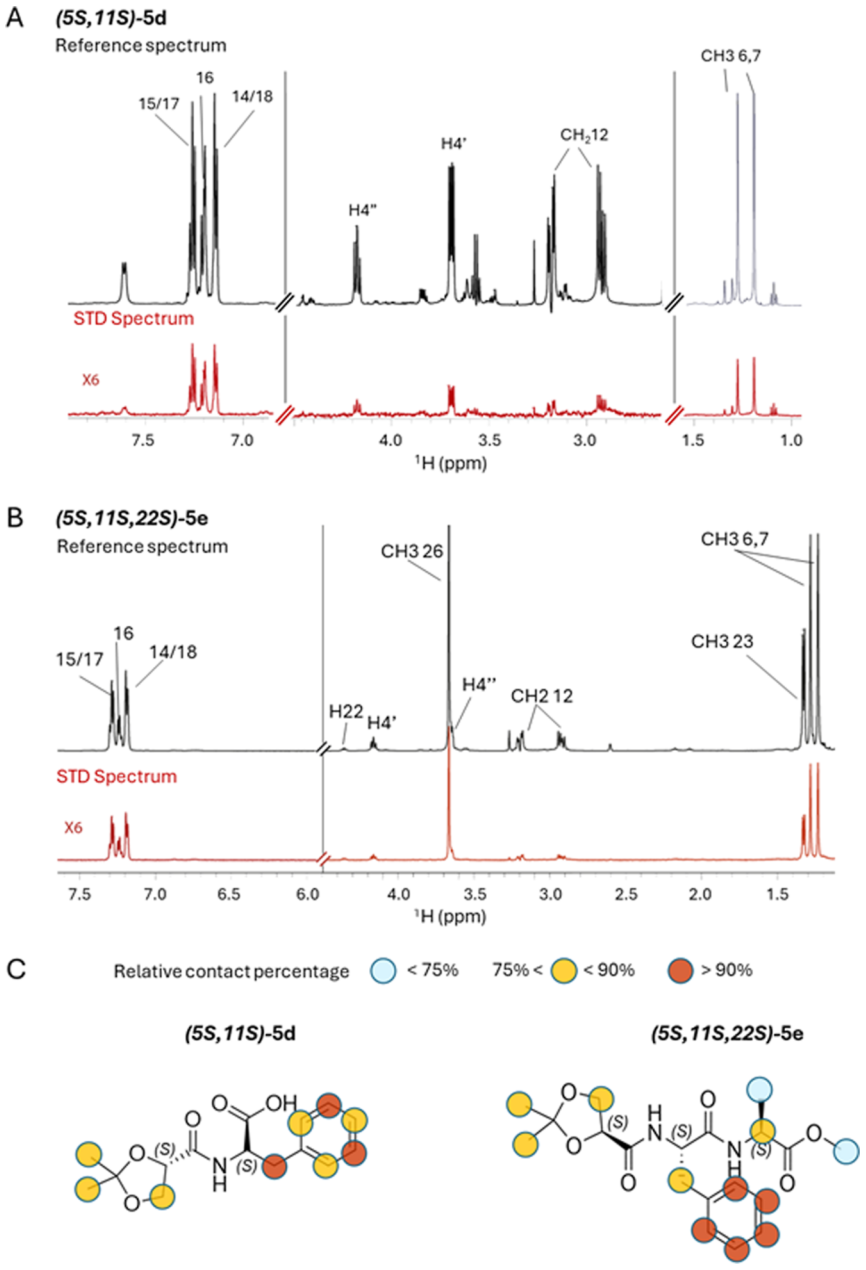

Figure 9. Selected regions of the reference (black) and STD NMR difference spectrum recorded at t_{sat} = 6 s (red) on (5*S*,11*S*)-**5d**/LsrK and (5*S*,11*S*,22*S*)-**5e**/LsrK 40:1 sample are reported in (A,B), respectively. Protons giving rise to STD signal are labeled on the reference spectrum (see Figure S9 of Supporting Information for proton numbering). An amplification factor was applied (×6) on STD spectra to optimize the visualization. (C) Binding epitope mapping from STD NMR data for the interaction of (5*S*,11*S*)-**5d** (left) and (5*S*,11*S*,22*S*)-**5e** (right) with LsrK. Protons are colored according to STD relative contact percentage (color code as reported on the figure).

study can inhibit biofilm formation by specifically targeting the AI-2 signaling pathway. This set our QSIs apart from other known QSIs, which often inhibit species-specific QS machinery or interfere with biofilm formation through more generalized and nonspecific mechanisms. Unlike species-specific QSIs that are highly effective but limited to certain bacterial species, the AI-2 pathway is a universal signaling mechanism involved in QS across both Gram-positive and Gram-negative bacteria. Thus, these QSIs may disrupt QS in a broader range of bacterial species and be effective against a wide range of pathogens. Looking forward, integrating QSIs that target the AI-2 pathway into therapeutic regimens could provide a novel strategy to combat AMR. Such QSIs offer a promising and innovative approach to addressing the challenges of complicated infections and AMR, becoming part of the arsenal against persistent and resistant bacterial infections.

EXPERIMENTAL SECTION

Chemistry. *General Procedures.* All commercially available chemicals and solvents were reagent grade and were used without further purification unless otherwise specified. Reactions were monitored by thin-layer chromatography on silica gel plates (60F-254, E. Merck) and visualized with UV light, cerium ammonium sulfate, or alkaline $KMnO_4$ aqueous solution. The following solvents and reagents have been abbreviated: ethyl ether (Et_2O), dimethyl sulfoxide (DMSO), ethyl acetate (EtOAc), dichloromethane (DCM), and methanol (MeOH). All reactions were carried out using standard

https://doi.org/10.1021/acs.jmedchem.4c01266
J. Med. Chem. 2024, 67, 18139−18156

techniques. NMR spectra were recorded on a Bruker 400 spectrometer with ^{1}H at 400.134 MHz and ^{13}C at 100.62 MHz. Proton chemical shift was referenced to the residual solvent peak. Chemical shifts are reported in parts per million (ppm and δ units). Coupling constants are reported in units of Hertz (Hz). Splitting patterns are designated as follows: s, singlet; d, doublet; t, triplet; q quartet; dd, double doublet; m, multiplet; b, broad. The purity of the final compounds was assessed by UPLC-UV-ESI/MS. Analyses were carried out on a JASCO system composed of an MD-2010 plus photodiode array detector, AS-4050 autosampler, and PU-4185 Binary pump. Analyses were run on a Symmetry C-18 (3.9 mm × 150 mm, 5 μm) column at 25 °C with a gradient elution solvent A, water containing 0.1% of formic acid; solvent B, methanol containing 0.1% of formic acid; gradient: 10% B to 90% B in 12 min, followed by isocratic elution 90% B for 2 min, with return to the initial conditions in 1 min at a flow rate of 1 mL/min. The chromatograms were recorded at 220 nm wavelength unless otherwise specified. All of the final synthesized compounds had 95% or higher purity. Optical rotation values were measured on a JASCO photoelectric polarimeter DIP 1000 with a 0.5 dm quartz cell at the sodium D line (λ = 589 nm); compounds were dissolved in methanol at a concentration of 0.5% (w/v), unless otherwise stated. Melting points were recorded on a Stuart, SMP3 (Barloworld Scientific Limited Stone, Staffordshire, UK) and are uncorrected.

*Synthesis of 1-((tert-Butyldimethylsilyl)oxy)but-3-yn-2-ol (**8**).* To a solution of 2-((*tert*-butyldimethylsilyl) oxy)acetaldehyde (1.0 equiv) in anhydrous THF, under nitrogen atmosphere and at −15 °C, ethynyl magnesium bromide 0.5 M in THF (1.1 equiv) was added. After 15 min, the reaction was quenched with a saturated solution of NH_4Cl and concentrated, and the residual aqueous phase was extracted with AcOEt. The organic layer was washed with brine, dried over anhydrous Na_2SO_4, filtered, and concentrated to yield the title compound which was used without further purification.

*Synthesis of But-3-yne-1,2-diol (**9**).* **8** (1.0 equiv) was dissolved in MeOH, and Amberlist-15 (100 mg per mmol) was added. The suspension was gently shaken overnight, filtered, and concentrated to give the title compound (quantitative yield) pure enough to be used in the next step without further purification.

*Synthesis of 2-Ethynyl-1,4-dioxaspiro[4.5]decane (**10**).* To a solution of 9 in anhydrous toluene, under nitrogen atmosphere and at room temperature, cyclohexanone (1.1 equiv) and a catalytic amount of pTSA were added. The solution was refluxed using a Dean−Stark trap to remove the forming water for 6 h and concentrated. The residue was suspended in AcOEt and washed with a saturated solution of Na_2CO_3 and brine, dried over anhydrous Na_2SO_4, filtered, and concentrated. The crude was purified over silica gel to give 234 mg (49% yield over three steps) of a pale-yellow liquid. ^{1}H NMR (400 MHz, $CDCl_3$): δ 4.64 (dd, 1H, J = 2.07, 6.31 Hz), 4.09 (dd, 1H, J = 6.31, 8.03 Hz), 3.87 (dd, 1H, J = 6.15, 8.03 Hz), 2.42 (d, 1H J = 2.07 Hz), 1.72−1.62 (m, 8H), 1.35−1.29 (m, 2H).

*Synthesis of 1-Phenyl-3-(1,4-dioxaspiro[4.5]decan-2-yl)prop-2-yn-1-one (**11**).* To a stirred solution of 10 (1.0 equiv) in anhydrous THF at room temperature and under nitrogen atmosphere were added $PdCl_2(PPh_3)_2$ (9% mol), CuI (3% mol), TEA (1.25 equiv), and benzoyl chloride (1.5 equiv), and the mixture was stirred at room temperature overnight. The mixture was filtered over a Celite aqueous medium and concentrated. The crude was redissolved in EtOAc and washed with water. The organic layer was dried over anhydrous Na_2SO_4, filtered, and concentrated to yield the title compound, which was used without further purification.

*Synthesis of 3-Phenyl-5-(1,4-dioxaspiro[4.5]decan-2-yl)-1H-pyrazole (**1**).* To a stirred solution of the 11 (1.0 equiv) in EtOH (2 mL) at room temperature, an aqueous solution of hydrazine (1.3 equiv) was added. The mixture was stirred at room temperature until starting material consumption and concentrated. The residue was dissolved in AcOEt and washed with a saturated solution of NH_4Cl and brine, dried over anhydrous Na_2SO_4, filtered, and concentrated. The crude was purified over silica gel to give 150 mg of a pale-yellow liquid (51% yield). ^{1}H NMR (400 MHz, $CDCl_3$): δ 7.67−7.31 (m, 5H), 6.56 (s, 1H), 5.22 (t, J = 6.4 Hz, 1H), 4.32 (t, J = 6.9 Hz, 1H), 3.99 (t, J = 7.5 Hz, 1H), 1.79−1.34 (m, 10H). Spectral characterization is in accordance with 36.

*Synthesis of 1-Methyl-3-phenyl-5-(1,4-dioxaspiro[4.5]decan-2-yl)-1H-pyrazole (**2**) and 1-Methyl-5-phenyl-3-(1,4-dioxaspiro[4.5]-decan-2-yl)-1H-pyrazole (**3**).* To a solution 1 (100 mg, 1.0 equiv) in anhydrous DMF, at room temperature and under nitrogen atmosphere, K_2CO_3 (2.5 equiv) was added. The mixture was stirred in the same conditions for 30 min. Thereafter, dimethylsulfate (1.0 equiv) was added, and the reaction was stirred at 60 °C overnight. The solvent was removed under reduced pressure, and the residue was redissolved in AcOEt. The organic phase was washed with a saturated solution of Na_2CO_3 and brine and dried over anhydrous Na_2SO_4, filtered, and concentrated. The crude was purified over silica gel to give 56 mg (52% yield) of 2 and 43 mg (40% yield) of 3, both as a pale-pearlash liquid.

*1-Methyl-3-phenyl-5-(1,4-dioxaspiro[4.5]decan-2-yl)-1H-pyrazole (**2**).* ^{1}H NMR (400 MHz, $CDCl_3$): δ 7.95 (ddd, J = 9.8, 6.0, 4.1 Hz, 6H), 7.62−7.54 (m, 6H), 7.51−7.42 (m, 4H), 6.70 (s, 1H), 5.37 (t, J = 6.3 Hz, 3H), 4.54 (dd, J = 8.3, 6.3 Hz, 3H), 4.27 (dd, J = 8.3, 7.0 Hz, 3H), 4.16 (s, 3H), 1.93−1.79 (m, 8H), 1.65−1.60 (m, 2H). Spectral characterization is in accordance with 36.

*1-Methyl-5-phenyl-3-(1,4-dioxaspiro[4.5]decan-2-yl)-1H-pyrazole (**3**).* ^{1}H NMR (400 MHz, $CDCl_3$): δ 7.−7.36 (m, 5H), 6.36 (s, 1H), 5.17 (dd, J = 7.7, 6.3 Hz, 1H), 4.32 (dd, J = 8.1, 6.3 Hz, 1H), 3.99 (t, J = 8.1 Hz, 1H), 3.84 (s, 3H), 1.78−1.59 (m, 10H). ESI-MS (m/z): calcd for $C_{18}H_{23}N_2O_2$ $[M + H]^+$, 299.2; found, 299.1.

*Synthesis of Potassium 2,2-Dimethyl-1,3-dioxolane-4-carboxylate (**14**).* To a solution of 2,2-dimethyl-1,3-dioxolane-4-methanol (5.0 g, 37.8 mmol, 1 equiv) in water (30 mL) at 0 °C was added KOH (3.2 g, 56.7 mmol, 1.5 equiv), and the mixture was stirred for a few minutes until dissolution. Thereafter, $KMnO_4$ (9.0 g, 56.7 mmol, 1 equiv) was added in portions over 15 min to avoid a temperature increase. Once the addition of $KMnO_4$ was concluded, the temperature was spontaneously raised, and the mixture was stirred at room temperature for 2 h. The reaction was quenched with methanol to reduce any residue $KMnO_4$, and the suspension was filtered over a Celite pad to remove the formed MnO_2. The pH of the filtrate was adjusted to 7 with concentrated sulfuric acid, and the solution concentrated. The residue was triturated with boiling ethanol and filtered to remove the K_2SO_4. The filtrate was concentrated, and the residue was triturated over diethyl ether. The precipitate was collected, washed with diethyl ether, and dried under vacuum to give 3.06 g of the title compounds as a white solid. The product is highly hygroscopic and must be stored under nitrogen and properly dried before use. White solid; 42% yield; ^{1}H NMR (400 MHz, D_2O): δ 4.57 (t, J = 7.2 Hz, 1H), 4.35 (t, J = 8.4, 1H), 3.98 (dd, J = 8.4, 7.2 Hz, 1H), 1.51 (s, 3H), 1.46 (s, 3H).

*Synthesis of (1,4-Dioxaspiro[4.5]decan-2-yl)methanol (**12**).* To a neat mixture of DL-1,2-Isopropylideneglycerol (1.32 g, 12.5 mmol, 1 equiv) and cyclohexanone (1.18 g, 12 mmol, 1 equiv) was added Amberlyst-15 (100 mg per mmol) was added. Reaction was stirred at 90 °C by distilling-off the formed acetone. After 2 h, the mixture was concentrated to evaporate the residual acetone. The crude was dissolved in diethyl ether, filtrated, and concentrated to give the title compound as a pale-yellow liquid pure enough to be directly used in the next step without further purification.

*Synthesis of Diethyl 2,2-Bis(hydroxymethyl)malonate (**15**).* To a suspension of $NaHCO_3$ (100 mg, 1.2 mmol, 0.1 equiv) in 30% aqueous formaldehyde (3.34 mL, 45 mmol, 3 equiv) was added the diethyl malonate (1.89 mL, 15 mmol, 1 equiv) dropwise, and the mixture was stirred overnight at room temperature. The reaction was quenched with a Na_2SO_4 saturated solution and extracted with ethyl acetate. The organic phase was dried with anhydrous Na_2SO_4, filtrated, and concentrated to give the title compound as a colorless liquid pure enough to be directly used in the next step without further purification. Colorless oil; 90% yield. ^{1}H NMR (400 MHz, $CDCl_3$): δ 4.26−4.17 (m, 4H), 4.08 (s, 4H), 1.29−1.18 (m, 6H).

*Synthesis of Diethyl 1,5-Dioxaspiro[5.5]undecane-3,3-dicarboxylate (**16**).* To a solution of 15 (7 g, 36 mmol, 1 equiv) in anhydrous toluene at room temperature and under nitrogen atmosphere,

https://doi.org/10.1021/acs.jmedchem.4c01266
J. Med. Chem. 2024, 67, 18139−18156

cyclohexanone (5.62 mL, 54 mmol, 1.5 equiv) and pTSA (720 mg, 3.6 mmol, 0.1 equiv) were added. The mixture was refluxed using a Dean-stark apparatus to trap the forming water for 2 h. Toluene was removed by vacuo, and the crude was solubilized in ethyl acetate and washed with 1 M HCl and a saturated solution of $NaHCO_3$. The organic layer was dried, filtered, and concentrated. The crude was purified by flash chromatography (ratio crude/silica gel 1:85; *n*-hexane/AcOEt 9:1) to give 4.5 g (37% yield) of a colorless oil. ^{1}H NMR (400 MHz, $CDCl_3$): δ 4.28 (s, 4H), 4.24 (q, J = 7.1 Hz, 4H), 1.75−1.73 (m, 4H), 1.59 (s, 2H), 1.55−1.48 (s, 4H), 1.27 (t, J = 7.1 Hz, 6H).

*Synthesis of 1,5-Dioxaspiro[5.5]undecane-3-carboxylic Acid (**17**).* **16** (1.32 g, 5 mmol, 1 equiv) was solubilized in a mixture of THF/EtOH 3:1, and 15 mL of a 1 M aqueous solution of KOH (841.5 mg, 15 mmol, 3 equiv) was added, and the reaction was stirred overnight at room temperature. After evaporating the organic phase, the aqueous solution was washed with AcOEt, acidified with 1 M HCl until pH < 7 and extracted with AcOEt. The organic phase was dried over anhydrous Na_2SO_4 and concentrated to give 1 g (93% yield) as a white solid which was solubilized in 20 mL of pyridine and refluxed for 3 h under nitrogen stream. The reaction mixture was cooled to room temperature, and the solvent removed in vacuo. The oily brown residue was dissolved in ethyl acetate, and the solution was washed with water. The solution was dried with Na_2SO_4, filtrated, and the solvent removed in vacuo to afford 705 mg (70% yield) of the titled compound as a white solid which was used in the next step without further purification. ^{1}H NMR (400 MHz, $CDCl_3$): δ 4.19−3.96 (m, 4H), 2.82−2.75 (m 1H), 1.83−1.75 (m, 2H), 1.75−1.67 (m, 2H), 1.57−1.44 (m, 4H), 1.42−1.37 (m, 2H).

*General Procedure for the Synthesis of Amides (**4a−c,e**, **5a−c,e**, and **7a−c,e**).* The appropriate carboxylic acid (13 for **4a−c**, **4d** for **4e**, 14 for **5a−c**, **5d** for **5e**, 17 for **7a−c,** and **7d** for **7e**, 1 equiv) was suspended in anhydrous DMF at 0 °C and under nitrogen atmosphere. EDC (1 equiv) and 1-hydroxybenzotriazole hydrate (HOBt) (1 equiv) were added followed by the addition of the appropriate amine (1.2 equiv) and TEA. The temperature was spontaneously raised, and the mixture was stirred at room temperature overnight. DMF was evaporated under vacuo, and the crude was resuspended in AcOEt. The organic phase was washed with 1 M HCl, a saturated solution of $NaHCO_3$, and brine. The organic phase was dried over anhydrous Na_2CO_3, filtered, and concentrated. The crude product was purified over silica gel.

*N-Benzyl-1,4-dioxaspiro[4.5]decane-2-carboxamide (**4a**).* LC conditions: crude/silica gel ratio 1:100, mobile phase: *n*-hexane/IPA 9:1. Yellow solid; mp [95−97 °C]. 66% yield. ^{1}H NMR (400 MHz, chloroform-*d*): δ 7.52−7.02 (m, 5H), 6.85 (s, 1H), 4.47 (dd, J = 7.6, 5.3 Hz, 1H), 4.41 (d, J = 6.0 Hz, 2H), 4.24 (t, J = 8.1 Hz, 1H), 4.07 (dd, J = 8.8, 5.2 Hz, 1H), 1.54 (dq, J = 15.4, 5.5, 4.6 Hz, 8H), 1.42−1.22 (m, 2H). ^{13}C NMR (100 MHz, $CDCl_3$): δ 171.36, 137.81, 128.78, 127.60, 127.53, 111.69, 74.78, 67.46, 42.95, 35.74, 34.39, 24.97, 23.98, 23.64. ESI-MS (m/z): calcd for $C_{16}H_{22}NO_3$ $[M + H]^+$, 276.2; found, 276.1.

*N-Phenethyl-1,4-dioxaspiro[4.5]decane-2-carboxamide (**4b**).* LC conditions: crude/silica gel ratio of 1:60, mobile phase: *n*-hexane/IPA of 9:1. Colorless liquid. 192 mg. 64% yield. ^{1}H NMR (400 MHz, chloroform-*d*): δ 7.32−7.12 (m, 5H), 6.55 (s, 1H), 4.36 (dd, J = 7.6, 5.2 Hz, 1H), 4.17 (t, J = 8.1 Hz, 1H), 3.95 (dd, J = 8.7, 5.2 Hz, 1H), 3.57 (dq, J = 13.3, 6.7 Hz, 1H), 3.43 (dp, J = 13.1, 6.9 Hz, 1H), 2.77 (td, J = 7.0, 3.2 Hz, 2H), 1.56−1.24 (m, 10H). ^{13}C NMR (101 MHz, $CDCl_3$) δ: 171.36, 138.49, 128.76, 128.71, 126.63, 111.54, 74.74, 67.44, 39.82, 35.60, 35.49, 34.34, 24.97, 23.95, 23.62. ESI-MS (m/z): calcd for $C_{17}H_{24}NO_3$ $[M + H]^+$, 290.2; found, 290.1.

*Methyl (1,4-Dioxaspiro[4.5]decane-2-carbonyl)-L-phenylalaninate (**4c**).* LC conditions: ratio crude/silica gel 1:100, mobile phase: *n*-hexane/IPA 9:1. A white waxy solid. 156 mg. 57% yield. ^{1}H NMR (400 MHz, $CDCl_3$): δ 7.39−7.24 (m, 3H), 7.15−7.09 (m, 3H), 4.87 (dtd, J = 7.9, 5.7, 1.3 Hz, 1H), 4.46 (dt, J = 7.6, 4.9 Hz, 1H), 4.25 (ddd, J = 8.7, 7.5, 2.8 Hz, 1H), 4.09 (dd, J = 8.8, 5.1 Hz, 0.5H), 3.97 (dd, J = 8.7, 5.2 Hz, 0.5H), 3.77 (s, 1.5H), 3.73 (s, 1.5H), 3.35−3.00 (m, 2H), 1.61−1.31 (m, 10H). ^{13}C NMR (101 MHz, $CDCl_3$): δ 171.61, 171.48, 171.24, 171.20, 135.57, 135.52, 129.28, 129.26, 128.67, 128.61, 127.24, 127.20, 111.87, 111.78, 74.72, 74.66, 67.36, 67.21, 52.57, 52.46, 52.44, 52.33, 37.95, 37.73, 35.45, 35.25, 34.62, 34.38, 24.98, 24.96, 23.93, 23.88, 23.70, 23.63. ESI-MS (m/z): calcd for $C_{19}H_{26}NO_5$ $[M + H]^+$, 348.2; found, 348.1.

*Methyl (1,4-Dioxaspiro[4.5]decane-2-carbonyl)-L-phenylalanyl-L-alaninate (**4e**).* LC conditions: ratio crude/silica gel 1:60, mobile phase: DCM/MeOH 9:1. Colorless liquid. 83% yield. ^{1}H NMR (400 MHz, $CDCl_3$): δ 7.51−7.01 (m, 6H), 6.42 (d, J = 7.3 Hz, 0.5H), 6.27 (d, J = 7.3 Hz, 0.5H), 4.60 (dq, J = 14.8, 7.2 Hz, 0.5H), 4.51−4.29 (m, 2H), 4.16 (dt, J = 16.0, 8.2 Hz, 1H), 4.09−3.93 (m, 0.5), 3.80 (dd, J = 8.9, 5.5 Hz, 1H), 3.66 (s, 1.5H), 3.64 (s, 1.5H), 3.06 (dddd, J = 48.4, 21.6, 14.1, 6.5 Hz, 2H), 1.60−1.40 (m, 6H), 1.40−1.29 (m, 7H). ^{13}C NMR (101 MHz, $CDCl_3$): δ 172.84, 172.71, 171.69, 171.56, 169.92, 169.74, 136.07, 136.00, 129.44, 129.30, 128.73, 128.65, 127.16, 127.10, 111.89, 111.86, 74.67, 74.62, 67.38, 67.22, 53.65, 53.50, 52.51, 52.48, 48.23, 48.14, 38.05, 37.98, 35.54, 35.41, 34.45, 34.32, 25.05, 25.03, 24.96, 24.94, 23.96, 23.95, 23.63, 18.27, 18.23. $[\alpha]_D$ −23.6° (c 0.5, MeOH).ESI-MS (m/z): calcd for $C_{22}H_{31}N_2O_6$ $[M + H]^+$, 419.2; found, 419.3.

*N-Benzyl-2,2-dimethyl-1,3-dioxolane-4-carboxamide (**5a**).* LC conditions: crude/silica gel ratio 1:100, mobile phase: *n*-hexane/AcOEt 7:3. A yellow solid; mp [96−98 °C]. 56% yield. ^{1}H NMR (400 MHz, $CDCl_3$): δ 7.34−7.05 (m, 5H), 6.91 (s, 1H), 4.38 (ddd, J = 20.2, 7.1, 4.1 Hz, 3H), 4.18 (td, J = 8.2, 3.1 Hz, 1H), 4.03 (ddd, J = 8.6, 5.3, 2.4 Hz, 1H), 1.34 (s, 3H), 1.28 (d, J = 2.1 Hz, 3H). ^{13}C NMR (101 MHz, $CDCl_3$): δ 171.19, 137.75, 128.81, 127.64, 127.58, 110.97, 75.08, 67.82, 42.97, 26.19, 25.01. ESI-MS (m/z): calcd for $C_{13}H_{18}NO_3$ $[M + H]^+$, 236.1; found, 236.1.

*2,2-Dimethyl-N-phenethyl-1,3-dioxolane-4-carboxamide (**5b**).* LC conditions: ratio crude/silica gel 1:100, mobile phase: *n*-hexane/AcOEt 7:3. Colorless liquid, 63% yield. ^{1}H NMR (400 MHz, $CDCl_3$): δ 7.32−6.98 (m, 5H), 6.60 (t, J = 6.0 Hz, 1H), 4.30 (dt, J = 7.3, 4.7 Hz, 1H), 4.12 (td, J = 8.2, 4.8 Hz, 1H), 3.91 (dt, J = 8.7, 4.4 Hz, 1H), 3.51 (ddt, J = 13.5, 6.8, 3.6 Hz, 1H), 3.34 (dt, J = 12.9, 5.7 Hz, 1H), 2.72 (ddt, J = 8.4, 6.6, 3.1 Hz, 2H), 1.21 (dd, J = 11.6, 3.4 Hz, 6H). ^{13}C NMR (101 MHz, $CDCl_3$): δ 170.14, 137.47, 127.73, 127.66, 125.60, 109.79, 73.99, 66.73, 38.87, 34.50, 24.94, 23.93. ESI-MS (m/z): calcd for $C_{14}H_{20}NO_3$ $[M + H]^+$, 250.1; found, 250.1.

*Methyl (2,2-Dimethyl-1,3-dioxolane-4-carbonyl)-L-phenylalaninate (**5c**).* LC conditions: ratio crude/silica gel 1:100, mobile phase: DCM/MeOH 95:5. Colorless liquid. 120 mg. 64% yield; ^{1}H NMR (400 MHz, $CDCl_3$): δ 7.32−7.11 (m, 3H), 7.04 (td, J = 7.2, 6.4, 1.8 Hz, 2H), 6.94 (d, J = 7.9 Hz, 1H), 4.80 (dtd, J = 8.4, 5.9, 2.1 Hz, 1H), 4.37 (ddd, J = 7.7, 5.0, 2.6 Hz, 1H), 4.17 (dd, J = 8.8, 7.6 Hz, 1H), 4.04 (dd, J = 8.8, 5.0 Hz, 0.5H), 3.87 (dd, J = 8.7, 5.2 Hz, 0.5H), 3.69 (d, J = 1.8 Hz, 1.5H), 3.65 (s, 1.5H), 3.25−2.96 (m, 2H), 1.32 (s, 1.5H), 1.31 (s, 1.5H), 1.28 (s, 1.5H), 1.22 (s, 1.5H). ^{13}C NMR (101 MHz, $CDCl_3$): δ 171.21, 171.13, 170.79, 170.66, 135.54 (2C), 129.00, 128.94, 128.36, 128.32, 126.89 (2C), 110.78, 110.70, 74.62, 74.55, 67.29, 67.15, 53.55 (2C), 52.16, 52.07, 37.38, 37.23, 25.60, 25.53, 24.95, 24.81. ESI-MS (m/z): calcd for $C_{16}H_{22}NO_5$ $[M + H]^+$, 308.1; found, 308.1.

*Methyl (2,2-Dimethyl-1,3-dioxolane-4-carbonyl)-L-phenylalanyl-L-alaninate (**5e**).* LC conditions: crude/silica gel ratio of 1:70, mobile phase: DCM/MeOH 95:5. A white solid; mp [79−81 °C]. 46% yield. ^{1}H NMR (400 MHz, chloroform-*d*): δ 7.35−7.19 (m, 5.5H), 7.10 (d, J = 8.0 Hz, 0.5H), 6.34 (d, J = 7.1 Hz, 0.5H), 6.21 (d, J = 7.6 Hz, 0.5H), 4.71−4.63 (m, 1H), 4.55−4.46 (m, 2H), 4.26 (dt, J = 13.3, 8.3 Hz, 1H), 4.17−4.12 (m, 0.5H), 3.89 (dd, J = 8.7, 5.6 Hz, 0.5H), 3.75 (s, 1.5H), 3.74 (d, J = 1.9 Hz, 1.5H), 3.25−3.03 (m, 2H), 1.41−1.33 (m, 9H). $[\alpha]_D^{25}$ −22.5° (c 0.5, MeOH). ESI-MS (m/z): calcd for $C_{19}H_{27}N_2O_6$ $[M + H]^+$, 379.4; found, 379.5.

*(5S,11S,22S)-Methyl (2,2-dimethyl-1,3-dioxolane-4-carbonyl)-L-phenylalanyl-L-alaninate ((5S,11S,22S)-**5e**).* A white solid, 68% yield. ^{1}H NMR (400 MHz, chloroform-*d*): δ 7.29−7.09 (m, 6H), 7.03 (d, J = 8.0 Hz, 1H), 6.34 (s, 1H), 4.61 (q, J = 7.3 Hz, 1H), 4.37 (dd, J = 7.6, 5.5 Hz, 1H), 4.15 (dd, J = 8.7, 7.6 Hz, 1H), 3.79 (dd, J = 8.7, 5.6 Hz, 1H), 3.66 (s, 3H), 3.04 (qd, J = 14.0, 7.0 Hz, 2H), 1.30

https://doi.org/10.1021/acs.jmedchem.4c01266
J. Med. Chem. 2024, 67, 18139−18156

(d, J = 7.2 Hz, 3H), 1.29−1.27 (m, 3H), 1.25−1.23 (m, 3H). ^{13}C NMR (101 MHz, $CDCl_3$): δ 172.81, 171.29, 169.84, 136.03, 129.31, 128.70, 127.16, 111.11, 74.91, 67.59, 53.57, 52.53, 48.25, 38.10, 25.88, 25.02, 18.27. $[\alpha]_D^{25}$ −32.5° (c 0.5, MeOH).

*(5R,11S,22S)-Methyl (2,2-Dimethyl-1,3-dioxolane-4-carbonyl)-L-phenylalanyl-L-alaninate ((5R,11S,22S)-**5e**).* A white solid, 72% yield. ^{1}H NMR (400 MHz, chloroform-d): δ 7.35−7.08 (m, 7H), 6.17 (s, 1H), 4.57 (ddd, J = 8.4, 7.3, 6.0 Hz, 1H), 4.39−4.33 (m, 1H), 4.18 (dd, J = 8.9, 7.5 Hz, 1H), 4.05 (dd, J = 8.9, 4.7 Hz, 1H), 3.64 (s, 3H), 3.13 (dd, J = 13.8, 5.9 Hz, 1H), 2.96 (dd, J = 13.8, 7.2 Hz, 1H), 1.32 (s, 3H), 1.30 (s, 3H), 1.25 (d, J = 7.1 Hz, 3H). ^{13}C NMR (101 MHz, $CDCl_3$): δ 172.69, 171.48, 169.68, 136.07, 129.42, 128.75, 127.20, 111.18, 74.98, 67.77, 53.68, 52.51, 48.18, 38.06, 26.01, 24.95, 18.31. $[\alpha]_D^{25}$ −12.3° (c 0.5, MeOH).

*N-Benzyl-1,5-dioxaspiro[5.5]undecane-3-carboxamide (**7a**).* LC conditions: ratio crude/silica gel 1:100, mobile phase: n-hexane/AcOEt 7:3. White solid; mp [84−86 °C]. 48% yield. ^{1}H NMR (400 MHz, $CDCl_3$): δ 7.28−7.19 (m, 5H), 7.00 (s, 1H), 4.45 (d, J = 5.7 Hz, 2H), 4.08 (ddd, J = 40.9, 12.3, 3.5 Hz, 4H), 2.33−2.31 (m, 1H), 1.80 (t, J = 6.0 Hz, 2H), 1.55−1.52 (m, 3H), 1.47−1.34 (m, 5H). ^{13}C NMR (101 MHz, $CDCl_3$): δ 172.89, 138.26, 128.67, 127.40, 127.35, 98.76, 60.47, 43.35, 41.78, 36.07, 29.03, 25.50, 22.34, 22.28. ESI-MS (m/z): calcd for $C_{17}H_{24}NO_3$ $[M + H]^+$, 290.2; found, 290.1.

*N-Phenethyl-1,5-dioxaspiro[5.5]undecane-3-carboxamide (**7b**).* LC conditions: ratio crude/silica gel 1:100, mobile phase: n-hexane/AcOEt 7:3. White solid; mp [108−110 °C]. 52% yield. ^{1}H NMR (400 MHz, $CDCl_3$): δ 7.25−7.21 (m, 4H), 7.16−7.12 (m, 1H), 7.07 (d, J = 8.0 Hz, 1H), 5.07 (p, J = 7.1 Hz, 1H), 4.06 (dd, J = 12.0, 3.8 Hz, 2H), 4.03−3.83 (m, 2H), 2.24 (t, J = 3.5 Hz, 1H), 1.79 (t, J = 5.9 Hz, 2H), 1.61−1.52 (m, 2H), 1.52−1.27 (m, 9H). ^{13}C NMR (101 MHz, $CDCl_3$): δ 172.81, 138.85, 128.81, 128.62, 126.48, 98.54, 60.39, 41.87, 40.48, 35.67, 35.61, 29.29, 25.52, 22.36, 22.33. ESI-MS (m/z): calcd for $C_{18}H_{26}NO_3$ $[M + H]^+$, 304.2; found, 304.1.

*Methyl (1,5-Dioxaspiro[5.5]undecane-3-carbonyl)-L-phenylalaninate (**7c**).* Colorless liquid. 160 mg. 91% yield. ^{1}H NMR (400 MHz, $CDCl_3$): δ 7.28−7.13 (m, 6H), 4.92 (dt, J = 7.6, 5.8 Hz, 1H), 4.09−4.05 (m, 1H), 3.97 (dddd, J = 13.6, 12.1, 3.8, 1.6 Hz, 2H), 3.73 (s, 3H), 3.28−3.07 (m, 2H), 2.34 (q, J = 4.0 Hz, 1H), 1.83 (d, J = 5.8 Hz, 2H), 1.61 (dd, J = 16.7, 9.7 Hz, 4H), 1.50 (dt, J = 11.3, 5.7 Hz, 2H), 1.41 (d, J = 7.3 Hz, 2H). ^{13}C NMR (101 MHz, $CDCl_3$): δ 172.39, 171.86, 135.88, 129.35, 128.52, 127.08, 98.63, 60.08, 53.19, 52.33, 41.72, 37.95, 35.28, 25.53, 22.33. ESI-MS (m/z): calcd for $C_{20}H_{27}NO_5$ $[M + H]^+$, 361.2; found, 361.2.

*Methyl (2,4-Dioxaspiro[5.5]undecane-3-carbonyl)-L-phenylalanyl-L-alaninate (**7e**).* LC conditions: ratio crude/silica gel 1:100, mobile phase: n-hexane/AcOEt 7:3. A white solid; mp [58−61 °C]. 32 mg. 86% yield. ^{1}H NMR (400 MHz, $CDCl_3$): δ 7.34 (d, J = 8.9 Hz, 1H), 7.30−7.06 (m, 5H), 6.84 (d, J = 8.1 Hz, 1H), 4.86−4.69 (m, 1H), 4.67−4.50 (m, 1H), 4.10 (ddd, J = 27.2, 12.3, 3.5 Hz, 2H), 4.02−3.75 (m, 2H), 3.63 (s, 3H), 3.26 (dd, J = 13.9, 5.9 Hz, 1H), 2.96 (dd, J = 13.9, 5.7 Hz, 1H), 2.27−2.16 (m, 1H), 1.74 (d, J = 34.4 Hz, 4H), 1.46−0.98 (m, 9H). ^{13}C NMR (101 MHz, $CDCl_3$): δ 173.23, 172.48, 170.32, 134.74, 128.39, 127.56, 126.10, 97.79, 59.46, 59.09, 58.95, 52.34, 40.39, 36.33, 34.39, 24.46, 21.28, 13.17. $[\alpha]_D^{25}$ −18.5° (c 0.8, MeOH). ESI-MS (m/z): calcd for $C_{23}H_{33}N_2O_6$ $[M + H]^+$, 433.2; found, 433.2.

*General Procedure for the Synthesis of Phenylalanine Derivatives (**4d, 5d and 7d**).* To a solution of the appropriate phenylalanine methyl ester derivative **4c**, **5c** or **7c** (1 equiv) in THF/MeOH 3:1, a 1 M aqueous solution of LiOH (1.1 equiv) was added. The mixture was stirred at room temperature for 1 h, and the organic solvent was removed under vacuo. The aqueous solution was washed with AcOEt and carefully acidified at pH < 3 with 1 M HCl. The aqueous solution was extracted with AcOEt, and the combined organic phase were washed with brine, dried over Na_2SO_4, filtered, and concentrated. The crude was purified over silica gel.

*(1,4-Dioxaspiro[4.5]decane-2-carbonyl)-L-phenylalanine (**4d**).* LC conditions: ratio crude/silica gel 1:100, mobile phase: DCM/MeOH 9:1. A yellowish solid; mp [116−117 °C]. 746 mg. 94% yield. ^{1}H NMR (400 MHz, $CDCl_3$): δ 7.27−7.08 (m, 5H), 7.00 (dd, J = 17.7, 7.9 Hz, 1H), 4.79 (qd, J = 7.9, 5.7 Hz, 1H), 4.39 (dd, J = 7.6, 5.1 Hz, 1H), 4.16 (td, J = 8.2, 5.9 Hz, 1H), 4.00 (dd, J = 8.8, 5.2 Hz, 0.5H), 3.88 (dd, J = 8.8, 5.1 Hz, 0.5H), 3.25−3.02 (m, 2H), 1.56−1.25 (m, 10H). ^{13}C NMR (101 MHz, $CDCl_3$): δ 174.36, 174.32, 172.08, 171.51, 135.39 (2C), 129.37 (2C), 128.76, 128.68, 127.33, 127.27, 112.00, 111.92, 74.54, 74.49, 67.27, 67.12, 52.60, 52.48, 37.36, 37.22, 35.37, 35.18, 34.48, 34.27, 24.95, 24.91, 23.92, 23.86, 23.66, 23.60. $[\alpha]_D^{25}$ 15.2° (c 0.5, MeOH). ESI-MS (m/z): calcd for $C_{18}H_{24}NO_5$ $[M + H]^+$, 334.2; found, 334.1.

*(2,2-Dimethyl-1,3-dioxolane-4-carbonyl)-L-phenylalanine (**5d**).* LC conditions: crude/silica gel ratio of 1:50, mobile phase: DMC/MeOH 9:1. A white solid; mp 102−104 °C 180 mg. 95% yield. ^{1}H NMR (400 MHz, $CDCl_3$): δ 7.27−7.08 (m, 5H), 7.03 (d, J = 8.3 Hz, 0.5H), 6.97 (d, J = 7.9 Hz, 0.5H), 4.81 (qd, J = 8.0, 7.5, 5.5 Hz, 1H), 4.39 (ddd, J = 7.1, 5.0, 1.7 Hz, 1H), 4.16 (ddd, J = 9.3, 7.6, 1.9 Hz, 1H), 4.02 (dd, J = 8.9, 4.9 Hz, 0.5H), 3.86 (dd, J = 8.8, 5.2 Hz, 0.5H), 3.31−3.01 (m, 2H), 1.29 (s, 1.5H), 1.28 (s, 1.5H), 1.27 (s, 1.5H), 1.18 (s, 1.5H). $[\alpha]_D^{25}$ + 22.8° (c 0.5, MeOH). ESI-MS (m/z): calcd for $C_{15}H_{20}NO_5$ $[M + H]^+$, 294.1; found, 294.1.

*(5S,11S)-(2,2-Dimethyl-1,3-dioxolane-5-carbonyl)-L-phenylalanine ((5S,11S)-**5d**).* A white solid. ^{1}H NMR (400 MHz, $CDCl_3$): δ 10.04 (s, 1H), 7.25−7.13 (m, 3H), 7.12−6.96 (m, 3H), 4.94−4.75 (m, 1H), 4.40 (dd, J = 7.6, 5.2 Hz, 1H), 4.15 (dd, J = 8.9, 7.6 Hz, 1H), 3.85 (dd, J = 8.8, 5.2 Hz, 1H), 3.22 (dd, J = 14.1, 5.4 Hz, 1H), 3.06 (dd, J = 14.1, 6.6 Hz, 1H), 1.26 (s, 3H), 1.18 (s, 3H). ^{13}C NMR (101 MHz, $CDCl_3$): δ 171.55, 170.94, 135.55, 129.28, 128.64, 127.24, 111.05, 74.92, 67.71, 52.53, 52.45, 37.83, 25.89, 24.95. $[\alpha]_D^{25}$ + 17.5° (c 0.5, MeOH).

*(5R,11S)-(2,2-Dimethyl-1,3-dioxolane-5-carbonyl)-L-phenylalanine ((5R,11S)-**5d**).* A white solid. ^{1}H NMR (400 MHz, chloroform-d): δ 8.84 (s, 1H), 7.37−7.15 (m, 3H), 7.16−7.06 (m, 2H), 7.02 (d, J = 8.3 Hz, 1H), 4.80 (dt, J = 8.2, 5.8 Hz, 1H), 4.38 (dd, J = 7.6, 5.0 Hz, 1H), 4.16 (dd, J = 8.9, 7.5 Hz, 1H), 4.02 (dd, J = 8.9, 5.0 Hz, 1H), 3.12 (dd, J = 6.1, 2.9 Hz, 2H), 1.29 (s, 3H), 1.28 (s, 3H). ^{13}C NMR (101 MHz, $CDCl_3$): δ 170.48, 170.11, 134.55, 128.21, 127.64, 126.22, 110.17, 73.97, 66.56, 51.49, 51.33, 36.92, 24.76, 24.13. $[\alpha]_D^{25}$ +29.4° (c 0.5, MeOH).

*(1,5-Dioxaspiro[5.5]undecane-3-carbonyl)-L-phenylalanine (**7d**).* Yellowish oil. 180 mg. 95% yield. ^{1}H NMR (400 MHz, $CDCl_3$): δ 7.30−7.18 (m, 6H), 4.87 (td, J = 7.1, 5.4 Hz, 1H), 4.06 (dd, J = 3.9, 1.8 Hz, 2H), 3.97−3.87 (m, 2H), 3.21 (ddd, J = 60.1, 14.0, 6.1 Hz, 2H), 2.36−2.34 (m, 1H), 1.88−1.85 (m, 2H), 1.50−1.36 (m, 8H). ^{13}C NMR (101 MHz, $CDCl_3$): δ 174.55, 173.75, 135.69, 129.38, 128.66, 127.20, 98.84, 60.14, 59.95, 41.48, 37.21, 35.81, 25.48, 22.31. ESI-MS (m/z): calcd for $C_{19}H_{26}NO_5$ $[M + H]^+$, 348.2; found, 348.2.

General Procedure for the Synthesis of the Diol Derivatives (6a−e). To a solution of the appropriate dimethyl ketal derivative **5a−e** in methanol/water 3:1, a catalytic amount of pTSA was added. The mixture was stirred at room temperature overnight, and the organic solvent was removed under vacuo. The aqueous solution was extracted with AcOEt, and the combined organic phase were washed with a saturated solution of Na_2CO_3 and brine. The organic phase was dried over anhydrous Na_2SO_4, filtered, and concentrated.

*N-Benzyl-2,3-dihydroxypropanamide (**6a**).* Colorless liquid. 67 mg. 98% yield. ^{1}H NMR (400 MHz, $CDCl_3$): δ 7.28−7.19 (m, 5H), 7.09 (br s, 1H), 4.39 (d, J = 5.9 Hz, 2H), 4.14 (t, J = 4.9 Hz, 1H), 3.81 (qd, J = 11.2, 4.9 Hz, 2H), 2.65 (s, 2H). ^{13}C NMR (100 MHz, chloroform-d): δ 172.82, 138.84, 128.29, 127.51, 127.48, 71.66, 63.49, 43.73. ESI-MS (m/z): calcd for $C_{10}H_{14}NO_3$ $[M + H]^+$, 196.1; found, 196.0.

*2,3-Dihydroxy-N-phenethylpropanamide (**6b**).* Colorless liquid. 87 mg. 63% yield. ^{1}H NMR (400 MHz, $CDCl_3$): δ 7.28−7.01 (m, 6H), 4.55−4.26 (m, 2H), 4.04 (q, J = 4.3, 3.3 Hz, 1H), 3.77−3.58 (m, 2H), 3.37 (q, J = 7.0 Hz, 2H), 2.69 (t, J = 7.4 Hz, 2H). ^{13}C NMR (101 MHz, $CDCl_3$): δ 171.78, 136.48, 127.72, 126.65, 126.60, 71.23, 63.21, 42.22, 28.70. ESI-MS (m/z): calcd for $C_{11}H_{16}NO_3$ $[M + H]^+$, 210.1; found, 210.1.

*Methyl (2,3-Dihydroxypropanoyl)-L-phenylalaninate (**6c**).* Colorless liquid. 176 mg, 84% yield. ^{1}H NMR (400 MHz, $CDCl_3$): δ 7.23−7.18 (m, 3H), 7.07−7.05 (m, 3H), 4.85−4.77 (m, 1H), 4.04 (ddd, J =

https://doi.org/10.1021/acs.jmedchem.4c01266
J. Med. Chem. 2024, 67, 18139−18156

7.1, 4.7, 2.1 Hz, 1H), 3.79 (dd, J = 11.4, 4.5 Hz, 1H), 3.67−3.3.62 (m, 4H), 3.14−3.09 (m, 1H), 3.05−2.97 (m, 1H). ^{13}C NMR (101 MHz, $CDCl_3$): δ 172.37, 172.16 (2C), 172.01, 135.68, 135.66, 129.26, 129.16, 128.72, 128.64, 127.29, 127.25, 72.34, 72.27, 64.19, 64.07, 53.09, 52.89, 52.63, 52.57, 37.90, 37.66. ESI-MS (m/z): calcd for $C_{13}H_{18}NO_5$ $[M + H]^+$, 268.1; found, 268.1.

*(2,3-Dihydroxypropanoyl)-L-phenylalanine (**6d**).* Whitish liquid, 36 mg, 57% yield. ^{1}H NMR (400 MHz, chloroform-d): δ 7.23−7.13 (m, 4H), 7.07−7.04 (m, 2H), 4.80 (dddd, J = 12.3, 8.1, 6.9, 5.6 Hz, 1H), 4.04 (td, J = 4.8, 3.4 Hz, 1H), 3.76 (dd, J = 11.4, 4.7 Hz, 1H), 3.70−3.66 (m, 1H), 3.13−2.97 (m, 2H). ^{13}C NMR (100 MHz, $CDCl_3$): δ 171.31, 171.11, 171.10, 170.97, 134.65, 134.63, 128.22, 128.12, 127.69, 127.61, 126.26, 126.22, 71.26, 71.19, 63.14, 63.03, 52.06, 51.86, 36.87, 36.63. ESI-MS (m/z): calcd for $C_{12}H_{16}NO_5$ $[M + H]^+$, 254.1; found, 254.1.

*Methyl (2,3-Dihydroxypropanoyl)-L-phenylalanyl-L-alaninate (**6e**).* A whitish solid. 62% yield. ^{1}H NMR (400 MHz, chloroform-d): δ 7.26−7.13 (m, 5.5H), 7.07 (d, J = 8.0 Hz, 0.5H), 6.43 (d, J = 6.8 Hz, 0.5H), 6.27 (d, J = 6.8 Hz, 0.5H), 4.85−4.76 (m, 1H), 4.47−4.36 (m, 2H), 4.16 (qnt, J = 8.4 Hz, 1H), 4.07−4.03 (m, 0.5H), 3.82−3.79 (m, 0.5H), 3.67 (s, 1.5H), 3.65 (s, 1.5H), 3.18−2.98 (m, 2H), 1.31 (d, J = 7.2 Hz, 1.5H), 1.25 (d, J = 7.2 Hz, 1.5H). ^{13}C NMR (100 MHz, chloroform-d): δ 172.92, 172.80, 171.77, 171.64, 170.01, 169.82, 136.08 (2C), 129.52, 129.39, 128.81, 128.73, 127.24, 127.181, 74.75, 74.71, 67.46, 67.31, 59.23, 59.31, 53.73, 53.59, 52.60, 52.56, 38.13, 38.07, 18.36, 18.31. ESI-MS (m/z): calcd for $C_{16}H_{23}N_2O_6$ $[M + H]^+$, 339.2; found, 339.1.

In Vitro Biological Assay. *Bacterial Strains and Culture Conditions.* The *P. aeruginosa* reference strain PA01 (laboratory collection) was grown in Luria Broth (LB) (VWR International S.r.l., Milan, Italy) containing 0.5% glucose at 37 °C with shaking. The *S. aureus* reference strain BH1CC (laboratory collection) was grown overnight in Brain Heart Infusion (BHI) broth (VWR International Srl) containing 2% glucose at 37 °C with shaking. *V. harveyi* strains (BAA-1116, BAA-1117, ATCC) (BAA-1118, ATCC) were grown overnight in Autoinducer Bioassay (AB) Medium at 30 °C with shaking. AB medium contained 0.3 M NaCl, 0.05 M $MgSO_4$, and 2% casamino acids, adjusted to pH 7.5 with 1 M NaOH. After autoclaving at 121 °C, 10 mL of 1 M potassium phosphate (1 M, pH 7.0), 10 mL of 0.1 M sterile arginine solution (L-Arg), and 10 mL of sterile glycerol were added to the medium (per 1 L).

S. aureus Biofilm Quantification Assay. An overnight bacterial culture in BHI medium, containing 0.5% glucose, was diluted 1:200 in fresh medium. 200 μL of the diluted bacterial suspension was added to 96-well flat-bottom sterile polystyrene microplates (Costar; Corning, New York, NY, USA) and incubated statically for 24 h at 37 °C in the presence or absence of inhibitors (2 to 500 μg/mL). The final DMSO concentration was 0.5%. Each well was softly washed twice with phosphate-buffered saline (PBS) (137 mM NaCl, 2.7 mM KCl, and 4.3 mM Na_2HPO_4 [pH 7.4]) to remove planktonic and loosely adhering bacteria. Therefore, adherent cells were exposed for 20 min to a solution of 25% formaldehyde (200 μL/well) to fix them onto the surface of each well and stained with 200 μL/well 0.5% crystal violet for 15 min, and after three washings, the wells were air-dried. For a quantitative estimation of the biofilm density, bound crystal violet was solubilized with 10% glacial acetic acid (200 μL/well), and the absorbance of the solubilized dye was read at 595 nm in a microplate reader (model 680; Bio-Rad Laboratories, Inc., Hercules, CA, USA).

P. aeruginosa Biofilm Quantification Assay. An overnight bacterial culture in LB medium, containing 2% of glucose, was diluted 1:100 in fresh medium. 200 μL of the culture was inoculated into the microtiter plate (Costar; Corning) and incubated for 2 h at 37 °C in the presence or absence of inhibitors (2 μg/mL to 500 μg/mL). The final DMSO concentration was 0.5%. After the incubation, the supernatant was removed and replaced with 200 μL of fresh medium. The plate was further incubated for 20 h at 37 °C. Each well was softly washed twice with PBS to remove planktonic and loosely adhering bacteria. Biofilm biomass was then quantified by crystal violet staining, as reported above.

Time-Killing Assays. Overnight bacterial culture was diluted 1:100 in fresh medium (BHI + 0.5% glucose for *S. aureus*, LB + 2% glucose for *P. aeruginosa*), and 200 μL/well of bacterial suspension was transferred into a U-bottom 96-well plate (Costar; Corning) in the presence or absence of compounds. Assays were carried out using a CLARIOstar microplate reader (BMG Labtech GmbH, Ortenberg, Germany), measuring the OD_{600} of the cultures every 15 min for 20 h at 37 °C. To perform these experiments, a custom plate mode program was set up, with shaking for 900 s (orbital shaking at 300 rpm, with 3 mm of diameter) before each reading, to increase the oxygenation and maintain bacteria in suspension.

V. harveyi BAA-1116, BAA-1117 and BAA1118 Bioluminescence Inhibition Assay. Vibrio strains were grown in AB medium (16 h, 30 °C, shaking) to $OD_{600\ nm}$ = 1.5. The cells were diluted 1:500 in overnight bacterial growth supernatant. CFSs were prepared by centrifuging the culture at 4000 rpm for 15 min at 4 °C. The resulting supernatants were passed through 0.2 μm syringe filters. A volume of 100 μL/well of each diluted culture was added to a 96-well flat-bottom sterile polystyrene microplate (Costar; Corning, New York, NY, USA) in the presence or absence of test compounds (500 μg/mL).

The MICs of the compounds tested for Vibrio strains in AB medium was evaluated before proceeding with the anti-QS assay. 2-fold serial dilutions of the compounds were prepared into a U-bottom 96-well plate starting from 500 μg/mL. Bacteria were collected during the mid log phase of growth and diluted to have about 5×10^5 cfu/mL. The diluted culture was directly added to the diluted compounds into the 96-well plate and then incubated at 30 °C for 24 h. After the incubation, 30 μL of 0.01% resazurin (Sigma-Aldrich) was added to each well, and the plate was further incubated at 30 °C for 4 h. Blue to purple resazurin is reduced to pink resorufin by aerobic respiration of metabolically active bacterial cells, allowing the visual determination of the MICs.

Str7410 compound was used as positive control, and it was assessed at the concentration of 0.4 μM (corresponding to the IC_{50} in *V. harveyi* BB170 AI-2 QS inhibitor activity as reported by Jiang et al.).[47] The final DMSO concentration was 0.5%. The plate was incubated at 30 °C for 8 h, and then, the bioluminescence ($OD_{460\ nm}$) and cell density ($OD_{600\ nm}$) were measured using a ClarioStar reader. Bioluminescence values were normalized over cell density values, and bioluminescence levels of bacteria incubated with each compound were expressed as % of control (bacterial cells resuspended in overnight supernatant medium in the absence of compounds), set as 100%.

Ligand−Protein Binding Assays. *Expression and Purification of LsrK.* Culture was grown at 37 °C to an OD_{600} of 0.3, transferred to 22 °C, and grown to an OD_{600} of 0.9. Expression was subsequently induced with 0.1 mM isopropyl 1-thio-β-D-galactopyranoside (Inalco, Milan, Italy) for 9 h. Cells were harvested and resuspended in 25 mM potassium phosphate, pH 7.0, 50 mM NaCl, 10 mM β-mercaptoethanol, 1 mM $MgCl_2$, 2.5 μg mL^{-1} DNase, and protease inhibitors and lysed by sonication (70% amplitude, 12 × 30″ on/off, 1′30″ interval between sonication steps). The cell debris was removed by centrifugation, and proteins were purified from the supernatants by Ni + 2-affinity chromatography on a HiTrap chelating column (GE Healthcare, Buckinghamshire, UK). Protein purity was assessed by 12.5% SDS-PAGE and Coomassie Brilliant Blue staining. A bicinchoninic acid protein assay (Pierce, Rockford, IL, USA) was used to measure the concentrations of purified proteins.

Differential Scanning Fluorimetry. A CFX96TM real-time PCR machine (Bio-Rad) was used to perform thermal melting experiments. The increase in the fluorescence of the SYPRO Orange dye (Sigma-Aldrich) as the protein thermally unfolded was measured. The excitation and emission filters for the SYPRO Orange dye were set to 470 and 570 nm, respectively. LsrK was prepared in the storage buffer as 22 μM stock solutions. 10 μL of protein was mixed with 1 μL of SYPRO Orange 125× and 1 μL of the 12.5 mM solution of tested compounds or 10 μL of the 1% DMSO solution in the protein storage buffer. The resulting mixture was diluted with 12.5 μL of protein storage buffer. The final reaction volume of 25 μL contained 5 μM

https://doi.org/10.1021/acs.jmedchem.4c01266
J. Med. Chem. 2024, 67, 18139−18156

protein, 5× Sypro Orange, and 1 mM tested compound. The heating gradient started at 25 °C; the temperature increased by 0.2/10 s until 95 °C, and the fluorescence of SYPRO Orange was read at each interval. Raw data files with temperatures and their corresponding fluorescence values (or first derivative of the fluorescence $-dF/dT$) were exported to Microsoft Office Excel, where melting temperature T_m from the lowest point of the first derivative plot was calculated. GraphPad Prism software was used to visualize the melting curves. Thermal shift values (ΔT_m) were obtained by subtracting the unfolding temperature of the LsrK in the presence of 2% (v/v) DMSO (TmDMSO) from the unfolding temperatures of the LsrK in the presence of the tested compounds.

Intrinsic Tryptophan Fluorescence. Fluorescence quenching experiments were carried out on a JASCO spectrofluorometer (FP-6200) using a 10 mm quartz cuvette. The temperature was maintained at 25 ± 0.1 °C by an external thermostated Peltier device. Stock solution of ligands was prepared in DMSO and working solution at the appropriate concentration were prepared in PBS. Protein aliquots (1.0 μM) were independently added with increasing concentrations of ligand, and the fluorescence emission spectrum was recorded in the range of 310−400 nm by keeping the excitation wavelength constant at 295 nm. The excitation and emission slit widths were kept at 2 nm. The final spectra were obtained by subtracting with the corresponding blank. For data analysis, the fluorescence intensity at λ_{max} was plotted against [ligand, μM].

Circular Dichroism. Far-UV (185−250 nm) CD measurements were performed at 20 °C in a 0.1 cm path length quartz cuvette. CD spectra were recorded on a JASCO J-720 spectropolarimeter. Appropriate blanks corresponding to the compound in the buffer were subtracted to the acquired induced CD spectra. The results are expressed as the mean residue ellipticity (MRE in deg cm^2 dmol^{-1} res^{-1}), which is defined by the following equation

$$\mathrm{MRE} = \frac{\text{observed CD}}{C_p \cdot n \cdot l \cdot 10}$$

where n is the number of amino acid residues (530 for LsrK), l is the path length of the cell (0.1 cm), and C_p is the molar (M) concentration of the protein. All the spectroscopic measurements were performed in nonsaline 20 mM phosphate buffer pH 7.4. Six scans were averaged for each spectrum.

NMR Interaction Studies. All samples were prepared in 50 mM phosphate buffer, pH 7.4, NaCl 100 mM, and DMSO 0.5% (v/v). All NMR experiments were performed at 25 °C on a 600 MHz Bruker NEO spectrometer equipped with a Prodigy cryoprobe. ^{1}H resonance assignment for ligands was performed via 1D ^{1}H NMR, 2D ^{1}H−^{1}H TOCSY, and ^{1}H−^{1}H ROESY experiments.

1D ^{1}H spectra were recorded on LsrK/**7b** samples at 1:0, 1:2, and 1:5 stoichiometric ratios with 1024 scans and D1 relaxation delay of 1 s. Water suppression was achieved by using excitation sculpting with gradients.

STD NMR experiments were performed on (5*S*,11*S*)-**5d** and (5*S*,11*S*,22*S*)-**5e** compounds. Samples were prepared using a ligand/protein ratio of 40:1. LsrK was dissolved 30 μM in the same buffer condition. STD NMR build-up curves were acquired at different saturation times (0.5, 0.75, 1, 1.5, 2, 3, and 6 s for (5*S*,11*S*)-**5d** ligand and 0.5, 0.75, 1, 1.5, 2, 3, 4, 5, and 6 s for (5*S*,11*S*,22*S*)-**5e** ligand). Irradiation frequencies were −0.385 and −40 ppm for the on-resonance and the off-resonance spectra, respectively. Cascades of 50 ms Gaussian-shaped pulses at a field strength of 50 Hz were employed with a delay of 1 ms between successive pulses. Protein signals were removed using a 25 ms spinlock filter (as implemented in the Bruker sequence stddiff.3). D1 relaxation delay was set to 6 s. Water suppression was achieved using excitation sculpting with gradients. All spectra were manually phased and baseline corrected using TOPSPIN 4.3.0 (Bruker, Karlsruhe, Germany).

Fractional STD effects were calculated at each saturation time (t_{sat}) by dividing signal intensity in the STD spectrum for the respective signals in the reference spectrum as follows: $(I_0 - I_{sat})/I_0$, where I_0 is the intensity of one signal in the off-resonance or reference NMR spectrum and I_{sat} is the intensity of the same signal in the on-resonance NMR STD spectrum. Build-up curves were fitted to a monoexponential function as in eq 1

$$\mathrm{STD}(t_{sat}) = \mathrm{STD}^{max}(1 - e^{-k_{sat}t_{sat}}) \quad (1)$$

where STD^{max} represents the maximum of the curve, k_{sat} is a rate constant, in s^{-1}, and t_{sat} is the saturation time, in seconds. Errors on STDmax and k_{sat} were derived from global fitting analysis (Sigmaplot 12.0 software) of STD build-up curves of split resonances belonging to the same proton. The initial slope STD0 of the curves was obtained as the product of the STDmax and k_{sat} coefficients. To map the main contact of the ligands to LsrK, STD0 values were normalized within a given ligand by the highest value, to which an arbitrary value of 100% was assigned.

■ ASSOCIATED CONTENT

Data Availability Statement

The raw data that support Figure 5 are available from the corresponding authors upon request. Data will be made available on request.

Supporting Information

The Supporting Information is available free of charge at https://pubs.acs.org/doi/10.1021/acs.jmedchem.4c01266.

Biofilm inhibition activity for compounds **1**−**3**, **4a**−**e**, **5a**−**e**, **6a**−**e**, and **7a**−**e** in *S. aureus* and *P. aeruginosa*; comparison of the percentages of secondary structural components in LsrK calculated by deconvolution of the CD spectrum and derived from the crystallographic structure; superimposition of the NMR spectra in the region 5.0−2.5 ppm of compounds (5*S*,11*S*)-**5d**, (5*R*,11*S*)-**5d**; superimposition of the NMR spectra in the region 5.0−2.5 ppm of compounds (5*S*,11*S*,22*S*)-**5e**, (5*R*,11*S*,22*S*)-**5e**; *S. aureus* time-killing assays in the presence or absence of the indicated compounds; *P. aeruginosa* time-killing assays in the presence or absence of the indicated compounds; superimposition of the experimental LsrK CD spectrum and the calculated ones obtained based on the estimation of the secondary structure using BestSel utility; 1D ^{1}H NMR line broadening of **7b** resonances in the presence of LsrK; STD-NMR build−up curves obtained for (5*S*,11*S*)-**5d** and (5*S*,11*S*,22*S*)-**5e** aromatic protons in the presence of LsrK; and ^{1}H and ^{13}C NMR spectra of compounds **4a**−**e**, **5a**−**e**, **6a**−**e**, and **7a**−**e** (PDF)

■ AUTHOR INFORMATION

Corresponding Authors

Giampiero Pietrocola − *Department of Molecular Medicine, Biochemistry Unit, University of Pavia, Pavia 27100, Italy;* orcid.org/0000-0002-7069-8155; Email: giampiero.pietrocola@unipv.it

Pasquale Linciano − *Department of Drug Sciences, University of Pavia, Pavia 27100, Italy;* orcid.org/0000-0003-0382-7479; Email: pasquale.linciano@unipv.it

Authors

Giorgio Milli − *Department of Drug Sciences, University of Pavia, Pavia 27100, Italy*

Angelica Pellegrini − *Department of Molecular Medicine, Biochemistry Unit, University of Pavia, Pavia 27100, Italy*

Roberta Listro − *Department of Drug Sciences, University of Pavia, Pavia 27100, Italy;* orcid.org/0000-0001-7615-1284

Marina Fasolini − *Nerviano Medical Sciences s.r.l., Nerviano, Milano 20014, Italy*
Katiuscia Pagano − *NMR Laboratory, Istituto di Scienze e Tecnologie Chimiche "Giulio Natta", CNR, Milano 20133, Italy;* orcid.org/0000-0002-0462-2056
Laura Ragona − *NMR Laboratory, Istituto di Scienze e Tecnologie Chimiche "Giulio Natta", CNR, Milano 20133, Italy;* orcid.org/0000-0003-3893-7117
Simona Collina − *Department of Drug Sciences, University of Pavia, Pavia 27100, Italy;* orcid.org/0000-0002-2954-7558

Complete contact information is available at: https://pubs.acs.org/10.1021/acs.jmedchem.4c01266

Author Contributions

The manuscript was written through contributions of all authors. All authors have given approval to the final version of the manuscript.

Notes

The authors declare no competing financial interest.

■ ACKNOWLEDGMENTS

This research was funded by the Italian University Ministry Project "ONE HEALTH BASIC AND TRANSLATIONAL RESEARCH ACTIONS (INF-ACT)" grant number PE13_INFACT_PNRR-U.A. 14.01, CUP F13C22001220007 to S.C. and EU funding within the NextGeneration EU-MUR PNRR Extended Partnership initiative on Emerging Infectious Diseases (project no. PE00000007, INF-ACT) to G.P. and by the Italian PRIN2022 (Progetti di Ricerca di Interesse Nazionale 2022) Project "LIRA:LsrK as Innovative molecular target for QS interfering agents for fighting Resistance to Antimicrobials" grant number 2022BCRZK2, CUP F53D23005050006 to P.L.

■ ABBREVIATIONS

AI-2,autoinducer-2; AMR,antimicrobial resistance; CD,circular dichroism; DPD,4,5-dihydroxy-2,3-pentanedione; DSF,differential scanning fluorimetry; EDC,1-ethyl-3-(3-(dimethylamino)propyl) carbodiimide; HOBt,hydroxybenzotriazole; ITF,intrinsic tryptophan fluorescence spectroscopy; LuxS,AI-2 synthase or *S*-ribosylhomocysteinase; $MBIC_{50}$,minimal biofilm inhibition concentration 50%; NAC,*N*-acetyl cysteine; Pfs,*S*-adenosylhomocysteine nucleosidase; pTSA,*para*-toluene sulfonic acid; QS,quorum sensing; QSI,quorum sensing inhibitor; *R*- or *S*-DHMF,,*R*- or *S*-2,4-dihydroxy-2-methyldihydro-3-furanone; *R*- or *S*-THMF,*R*- or *S*-2-methyl-2,3,3,4-tetrahydroxytetrahydrofuran; SAH,*S*-adenosylhomocysteine; SAM,*S*-adenosylmethionine; SRH,*S*-ribosylhomocysteine; STD-NMR,saturation transfer differences-NMR

■ REFERENCES

(1) Salam, M. A.; Al-Amin, M. Y.; Salam, M. T.; Pawar, J. S.; Akhter, N.; Rabaan, A. A.; Alqumber, M. A. A. Antimicrobial Resistance: A Growing Serious Threat for Global Public Health. *Healthcare* **2023**, *11* (13), 1946.
(2) World Health Organization. *Global Antimicrobial Resistance and Use Surveillance System (GLASS) Report 2022*, 2022.
(3) Darby, E. M.; Trampari, E.; Siasat, P.; Gaya, M. S.; Alav, I.; Webber, M. A.; Blair, J. M. A. Molecular Mechanisms of Antibiotic Resistance Revisited. *Nat. Rev. Microbiol.* **2023**, *21* (5), 280−295.
(4) Linciano, P.; Cendron, L.; Gianquinto, E.; Spyrakis, F.; Tondi, D. Ten Years with New Delhi Metallo-β-lactamase-1 (NDM-1): From Structural Insights to Inhibitor Design. *ACS Infect. Dis.* **2019**, *5* (1), 9−34.
(5) Balducci, E.; Papi, F.; Capialbi, D. E.; Del Bino, L. Polysaccharides' Structures and Functions in Biofilm Architecture of Antimicrobial-Resistant (AMR) Pathogens. *Int. J. Mol. Sci.* **2023**, *24* (4), 4030.
(6) Du Toit, A. Bacterial Architects Build the Biofilm Structures. *Nat. Rev. Microbiol.* **2024**, *22* (4), 187.
(7) Gondil, V. S.; Subhadra, B. Biofilms and Their Role on Diseases. *BMC Microbiol.* **2023**, *23* (1), 203.
(8) Vestby, L. K.; Grønseth, T.; Simm, R.; Nesse, L. L. Bacterial Biofilm and Its Role in the Pathogenesis of Disease. *Antibiotics* **2020**, *9* (2), 59.
(9) Pang, Z.; Raudonis, R.; Glick, B. R.; Lin, T.-J.; Cheng, Z. Antibiotic Resistance in Pseudomonas Aeruginosa: Mechanisms and Alternative Therapeutic Strategies. *Biotechnol. Adv.* **2019**, *37* (1), 177−192.
(10) Lee, J.; Zhang, L. The Hierarchy Quorum Sensing Network in Pseudomonas Aeruginosa. *Protein Cell* **2015**, *6* (1), 26−41.
(11) Taylor, P. K.; Yeung, A. T. Y.; Hancock, R. E. W. Antibiotic Resistance in Pseudomonas Aeruginosa Biofilms: Towards the Development of Novel Anti-Biofilm Therapies. *J. Biotechnol.* **2014**, *191*, 121−130.
(12) Ciofu, O.; Tolker-Nielsen, T. Tolerance and Resistance of Pseudomonas Aeruginosa Biofilms to Antimicrobial Agents—How P. Aeruginosa Can Escape Antibiotics. *Front. Microbiol.* **2019**, *10*, 913.
(13) Mukherjee, S.; Bassler, B. L. Bacterial Quorum Sensing in Complex and Dynamically Changing Environments. *Nat. Rev. Microbiol.* **2019**, *17* (6), 371−382.
(14) Papenfort, K.; Bassler, B. L. Quorum Sensing Signal−Response Systems in Gram-Negative Bacteria. *Nat. Rev. Microbiol.* **2016**, *14* (9), 576−588.
(15) Boban, T.; Nadar, S.; Tauro, S. Breaking down Bacterial Communication: A Review of Quorum Quenching Agents. *Futur J. Pharm. Sci.* **2023**, *9* (1), 77.
(16) Papenfort, K.; Bassler, B. L. Quorum Sensing Signal-Response Systems in Gram-Negative Bacteria. *Nat. Rev. Microbiol.* **2016**, *14* (9), 576−588.
(17) Mukherjee, S.; Bassler, B. L. Bacterial Quorum Sensing in Complex and Dynamically Changing Environments. *Nat. Rev. Microbiol.* **2019**, *17* (6), 371−382.
(18) Zhang, L.; Li, S.; Liu, X.; Wang, Z.; Jiang, M.; Wang, R.; Xie, L.; Liu, Q.; Xie, X.; Shang, D.; Li, M.; Wei, Z.; Wang, Y.; Fan, C.; Luo, Z.-Q.; Shen, X. Sensing of Autoinducer-2 by Functionally Distinct Receptors in Prokaryotes. *Nat. Commun.* **2020**, *11* (1), 5371.
(19) Vendeville, A.; Winzer, K.; Heurlier, K.; Tang, C. M.; Hardie, K. R. Making "sense" of Metabolism: Autoinducer-2, LuxS and Pathogenic Bacteria. *Nat. Rev. Microbiol.* **2005**, *3* (5), 383−396.
(20) Xavier, K. B.; Bassler, B. L. Regulation of Uptake and Processing of the Quorum-Sensing Autoinducer AI-2 in Escherichia Coli. *J. Bacteriol.* **2005**, *187* (1), 238−248.
(21) Miller, S. T.; Xavier, K. B.; Campagna, S. R.; Taga, M. E.; Semmelhack, M. F.; Bassler, B. L.; Hughson, F. M. Salmonella Typhimurium Recognizes a Chemically Distinct Form of the Bacterial Quorum-Sensing Signal AI-2. *Mol. Cell* **2004**, *15* (5), 677−687.
(22) Xavier, K. B.; Bassler, B. L. Interference with AI-2-Mediated Bacterial Cell-Cell Communication. *Nature* **2005**, *437* (7059), 750−753.
(23) Li, J.; Attila, C.; Wang, L.; Wood, T. K.; Valdes, J. J.; Bentley, W. E. Quorum Sensing in Escherichia Coli Is Signaled by AI-2/LsrR: Effects on Small RNA and Biofilm Architecture. *J. Bacteriol.* **2007**, *189* (16), 6011−6020.
(24) Guo, M.; Gamby, S.; Zheng, Y.; Sintim, H. Small Molecule Inhibitors of AI-2 Signaling in Bacteria: State-of-the-Art and Future Perspectives for Anti-Quorum Sensing Agents. *Int. J. Mol. Sci.* **2013**, *14* (9), 17694−17728.

(25) Ha, J.-H.; Eo, Y.; Grishaev, A.; Guo, M.; Smith, J. A. I.; Sintim, H. O.; Kim, E.-H.; Cheong, H.-K.; Bentley, W. E.; Ryu, K.-S. Crystal Structures of the LsrR Proteins Complexed with Phospho-AI-2 and Two Signal-Interrupting Analogues Reveal Distinct Mechanisms for Ligand Recognition. *J. Am. Chem. Soc.* **2013**, *135* (41), 15526−15535.
(26) Li, J.; Attila, C.; Wang, L.; Wood, T. K.; Valdes, J. J.; Bentley, W. E. Quorum Sensing in Escherichia Coli Is Signaled by AI-2/LsrR: Effects on Small RNA and Biofilm Architecture. *J. Bacteriol.* **2007**, *189* (16), 6011−6020.
(27) Wang, Y.; Liu, B.; Grenier, D.; Yi, L. Regulatory Mechanisms of the LuxS/AI-2 System and Bacterial Resistance. *Antimicrob. Agents Chemother.* **2019**, *63* (10), No. e01186.
(28) Linciano, P.; Cavalloro, V.; Martino, E.; Kirchmair, J.; Listro, R.; Rossi, D.; Collina, S. Tackling Antimicrobial Resistance with Small Molecules Targeting LsrK: Challenges and Opportunities. *J. Med. Chem.* **2020**, *63* (24), 15243−15257.
(29) Vendeville, A.; Winzer, K.; Heurlier, K.; Tang, C. M.; Hardie, K. R. Making "sense" of Metabolism: Autoinducer-2, LUXS and Pathogenic Bacteria. *Nat. Rev. Microbiol.* **2005**, *3* (5), 383−396.
(30) Gatta, V.; Tomašič, T.; Ilaš, J.; Zidar, N.; Peterlin Mašič, L.; Barančoková, M.; Frlan, R.; Anderluh, M.; Kikelj, D.; Tammela, P. A New Cell-Based AI-2-Mediated Quorum Sensing Interference Assay in Screening of LsrK-Targeted Inhibitors. *ChemBioChem* **2020**, *21*, 1918.
(31) Medarametla, P.; Gatta, V.; Kajander, T.; Laitinen, T.; Tammela, P.; Poso, A. Structure-Based Virtual Screening of LsrK Kinase Inhibitors to Target Quorum Sensing. *ChemMedChem* **2018**, *13* (22), 2400−2407.
(32) Gatta, V.; Ilina, P.; Porter, A.; McElroy, S.; Tammela, P. Targeting Quorum Sensing: High-Throughput Screening to Identify Novel Lsrk Inhibitors. *Int. J. Mol. Sci.* **2019**, *20* (12), 3112.
(33) Mao, Y.; Liu, P.; Chen, H.; Wang, Y.; Li, C.; Wang, Q. Baicalein Inhibits the Staphylococcus Aureus Biofilm and the LuxS/AI-2 System in Vitro. *Infect. Drug Resist.* **2023**, *16* (May), 2861−2882.
(34) Brackman, G.; Cos, P.; Maes, L.; Nelis, H. J.; Coenye, T. Quorum Sensing Inhibitors Increase the Susceptibility of Bacterial Biofilms to Antibiotics In Vitro and In Vivo. *Antimicrob. Agents Chemother.* **2011**, *55* (6), 2655−2661.
(35) Schütz, C.; Empting, M. Targeting the Pseudomonas Quinolone Signal Quorum Sensing System for the Discovery of Novel Anti-Infective Pathoblockers. *Beilstein J. Org. Chem.* **2018**, *14*, 2627−2645.
(36) Stotani, S.; Gatta, V.; Medarametla, P.; Padmanaban, M.; Karawajczyk, A.; Giordanetto, F.; Tammela, P.; Laitinen, T.; Poso, A.; Tzalis, D.; Collina, S. DPD-Inspired Discovery of Novel LsrK Kinase Inhibitors: An Opportunity to Fight Antimicrobial Resistance. *J. Med. Chem.* **2019**, *62* (5), 2720−2737.
(37) Gallo, M.; Matteucci, S.; Alaimo, N.; Pitti, E.; Orsale, M. V.; Summa, V.; Cicero, D. O.; Monteagudo, E. A Novel Method Using Nuclear Magnetic Resonance for Plasma Protein Binding Assessment in Drug Discovery Programs. *J. Pharm. Biomed. Anal.* **2019**, *167*, 21−29.
(38) Pagano, K.; Longhi, E.; Molinari, H.; Taraboletti, G.; Ragona, L. Inhibition of FGFR Signaling by Targeting FGF/FGFR Extracellular Interactions: Towards the Comprehension of the Molecular Mechanism through NMR Approaches. *Int. J. Mol. Sci.* **2022**, *23* (18), 10860.
(39) Lagorce, D.; Sperandio, O.; Baell, J.; Miteva, M.; Villoutreix, B. FAFDrugs4. http://fafdrugs4.mti.univ-paris-diderot.fr (accessed Oct 09, 2022).
(40) Linciano, P.; Pinzi, L.; Belluti, S.; Chianese, U.; Benedetti, R.; Moi, D.; Altucci, L.; Franchini, S.; Imbriano, C.; Sorbi, C.; Rastelli, G. Inhibitors of Histone Deacetylase 6 Based on a Novel 3-Hydroxy-Isoxazole Zinc Binding Group. *J. Enzyme Inhib. Med. Chem.* **2021**, *36* (1), 2080−2086.
(41) Franchini, S.; Sorbi, C.; Linciano, P.; Carnevale, G.; Tait, A.; Ronsisvalle, S.; Buccioni, M.; Del Bello, F.; Cilia, A.; Pirona, L.; Denora, N.; Iacobazzi, R. M.; Brasili, L. 1,3-Dioxane as a scaffold for potent and selective 5-HT1AR agonist with in-vivo anxiolytic, anti-depressant and anti-nociceptive activity. *Eur. J. Med. Chem.* **2019**, *176*, 310−325.
(42) Linciano, P.; Benedetti, R.; Pinzi, L.; Russo, F.; Chianese, U.; Sorbi, C.; Altucci, L.; Rastelli, G.; Brasili, L.; Franchini, S. Investigation of the Effect of Different Linker Chemotypes on the Inhibition of Histone Deacetylases (HDACs). *Bioorg. Chem.* **2021**, *106* (November 2020), 104462.
(43) Lima, E. M. F.; Almeida, F. A. d.; Sircili, M. P.; Bueris, V.; Pinto, U. M. N-Acetylcysteine (NAC) Attenuates Quorum Sensing Regulated Phenotypes in Pseudomonas Aeruginosa PAO1. *Heliyon* **2023**, *9* (3), No. e14152.
(44) Lima, E. M. F.; Almeida, F. A. d.; Sircili, M. P.; Bueris, V.; Pinto, U. M. N-Acetylcysteine (NAC) Attenuates Quorum Sensing Regulated Phenotypes in Pseudomonas Aeruginosa PAO1. *Heliyon* **2023**, *9* (3), No. e14152.
(45) Zheng, J.; Shang, Y.; Wu, Y.; Zhao, Y.; Chen, Z.; Lin, Z.; Li, P.; Sun, X.; Xu, G.; Wen, Z.; Chen, J.; Wang, Y.; Wang, Z.; Xiong, Y.; Deng, Q.; Qu, D.; Yu, Z. Loratadine Inhibits Staphylococcus Aureus Virulence and Biofilm Formation. *iScience* **2022**, *25* (2), 103731.
(46) Viering, B. L.; Balogh, H.; Cox, C. F.; Kirpekar, O. K.; Akers, A. L.; Federico, V. A.; Valenzano, G. Z.; Stempel, R.; Pickett, H. L.; Lundin, P. M.; Blackledge, M. S.; Miller, H. B. Loratadine Combats Methicillin-Resistant Staphylococcus Aureus by Modulating Virulence, Antibiotic Resistance, and Biofilm Genes. *ACS Infect. Dis.* **2024**, *10* (1), 232−250.
(47) Jiang, K.; Xu, Y.; Yuan, B.; Yue, Y.; Zhao, M.; Luo, R.; Wu, H.; Wang, L.; Zhang, Y.; Xiao, J.; Lin, F. Effect of Autoinducer-2 Quorum Sensing Inhibitor on Interspecies Quorum Sensing. *Front. Microbiol.* **2022**, *13*, 791802.
(48) Baljinnyam, B.; Ronzetti, M.; Yasgar, A.; Simeonov, A. Applications of Differential Scanning Fluorometry and Related Technologies in Characterization of Protein−Ligand Interactions. *Methods Mol. Biol.* **2020**, *2089*, 47−68.
(49) Niesen, F. H.; Berglund, H.; Vedadi, M. The Use of Differential Scanning Fluorimetry to Detect Ligand Interactions That Promote Protein Stability. *Nat. Protoc.* **2007**, *2* (9), 2212−2221.
(50) Zhu, J.; Hixon, M. S.; Globisch, D.; Kaufmann, G. F.; Janda, K. D. Mechanistic Insights into the LsrK Kinase Required for Autoinducer-2 Quorum Sensing Activation. *J. Am. Chem. Soc.* **2013**, *135* (21), 7827−7830.
(51) Listro, R.; Milli, G.; Pellegrini, A.; Motta, C.; Cavalloro, V.; Martino, E.; Kirchmair, J.; Pietrocola, G.; Rossi, D.; Linciano, P.; Collina, S. Structural Insights into the Ligand−LsrK Kinase Binding Mode: A Step Forward in the Discovery of Novel Antimicrobial Agents. *Molecules* **2023**, *28* (6), 2542.
(52) Micsonai, A.; Bulyáki, E.; Kardos, J. BeStSel: From Secondary Structure Analysis to Protein Fold Prediction by. Circular Dichroism Spectroscopy. *Methods Mol. Biol.* **2021**, *2199*, 175−189.
(53) Mayer, M.; Meyer, B. Group Epitope Mapping by Saturation Transfer Difference NMR To Identify Segments of a Ligand in Direct Contact with a Protein Receptor. *J. Am. Chem. Soc.* **2001**, *123* (25), 6108−6117.
(54) Mayer, M.; Meyer, B. Group Epitope Mapping by Saturation Transfer Difference NMR To Identify Segments of a Ligand in Direct Contact with a Protein Receptor. *J. Am. Chem. Soc.* **2001**, *123* (25), 6108−6117.

https://doi.org/10.1021/acs.jmedchem.4c01266
J. Med. Chem. 2024, 67, 18139−18156